

Bifurcation analysis of microscopic follow-the-leader traffic models

Dissertation
zur Erlangung des Doktorgrades
der Fakultät für Mathematik, Informatik
und Naturwissenschaften
der Universität Hamburg

vorgelegt
im Department Mathematik
von

Gabriele Sirito
aus Parma, Italien

Hamburg
2006

Als Dissertation angenommen vom Fachbereich
Mathematik der Universität Hamburg

auf Grund der Gutachten von Prof. Dr. I. Gasser
und Prof. Dr. B. Werner

Hamburg, den 2. Dezember 2005

Prof. Dr. A. Kreuzer
Dekan des Fachbereichs Mathematik

Contents

- 1 Introduction** **2**
- 1.1 Setting of the problem 5

- 2 Optimal velocity model** **9**
- 2.1 Linear analysis 9
- 2.2 Drivers with the same driving law: Hopf bifurcation 10
 - 2.2.1 Structure of the eigenvalues 12
 - 2.2.2 Bifurcation analysis 16
 - 2.2.3 Discussion for different optimal velocity functions . . . 18
- 2.3 Drivers with the same driving law: numerical bifurcation analysis 20
- 2.4 Perturbative argument for non-equal drivers 23

- 3 Aggressive drivers and variable reaction times** **28**
- 3.1 Linear and local bifurcation analysis 28
- 3.2 Numerical bifurcation analysis 32
 - 3.2.1 Aggressive drivers with constant reaction time 32
 - 3.2.2 The pure optimal velocity model with variable reaction
time 35
 - 3.2.3 The full model (3.1) 39

- 4 Conclusions** **41**

- A Calculation of a first Lyapunov coefficient** **43**

Chapter 1

Introduction

Traffic flow is an interesting phenomenon of our modern world. Although we all experience it daily, traffic flow is far from being well understood. It is a life science problem, since drivers do not usually act according to well defined rules. However, the increase of traffic in many areas and the related problems underline the importance of a realistic description of traffic flow or of some of its features.

The mathematical modeling of traffic flow has a long tradition. Various approaches can be found in literature. A very common class of traffic models is the macroscopic one, where the traffic flow is described in terms of density and velocity distributions. One of the earliest models of this kind is the “classical” Lighthill-Whitham model [21]. A second class of approaches consists of the kinetic Boltzmann-like models, where probability distribution functions of the traffic flow are considered [18]. In the eighties cellular automata models became popular and are still used. Yet another idea was that of regarding the formation of a traffic jam as a clustering phenomenon linked to a Markov process. This stochastic approach leads to the study of the master-equation for a particular probability distribution and can be found in works such as [22].

A very important class of models are the so called microscopic models, where the dynamics of the single cars is described. The earliest microscopic models were proposed in the early fifties in [27, 28, 29].

For an overview on the different modeling approaches see [6, 11, 12, 18].

The models considered in this paper are special class of microscopic models, the so called follow-the-leader models, where the dynamics of every car depends mainly on its distance to the car in front (called headway) and on the relative velocity with respect to the car in front. A historical overview on follow-the-leader models is given in [6].

In follow-the-leader models every car (or better its position) is described

by an ordinary differential equation. This equation defines deterministically the behavior of the car driver. It is assumed that there exists something like a “mean” driver, i.e. all drivers act according to some general law. Follow-the-leader models are easy to implement numerically. They not only show the dynamics of the single cars, but also some macroscopic behavior like the formation of more vs. less dense sections of the road. However the link between microscopic and macroscopic models is still a challenging problem (see [1, 20]). Finally how to choose an adequate microscopic model in order to obtain realistic macroscopic phenomena, is also still subject of debate (see [12]).

In this work I will consider follow-the-leader models on a circular road, which leads to an (in general big) autonomous system of ODE’s. These systems are known to have special (quasi stationary) solutions with constant headways and constant relative velocities. It is known that these solutions are stable up to a critical car-density [4, 13]. Especially in the last years there is a increased interest in the behavior beyond the critical density, i.e. in the region, where the quasi-stationary solution is unstable. A natural way to explore the dynamics beyond the critical density is bifurcation theory. In fact, a few authors based on numerical experiment have conjectured the existence of bifurcations [2, 15].

In my work together with I. Gasser, T. Seidel and B. Werner a systematic bifurcation analysis of different follow-the-leader models was conducted, leading to the two publications [8] and [9]. These two articles belong together in that the second one is the natural extension of the first one. This work wants to present the material in the two article in unitary form and formalism.

In [8] the standard optimal velocity models were analyzed. In these models we assume that the acceleration of each car depends on the difference between the car velocity and an “optimal” velocity, which models the velocity in an “equilibrium” situation for example as function of the headway (distance of a car to the car in front). Due to the high number of cars in real relevant traffic situations these models consist typically of big systems of nonlinear ODE’s.

Frequently used settings are an infinite single lane or N cars on a circle. The latter is considered from now on in this paper.

For realistic optimal velocity functions it is easy to see that these models allow a quasi-stationary state, i.e. a solution where all cars have the same velocity and a constant (in time) headway. A stability analysis shows that this solution is stable for certain parameter regimes ([2, 3, 4, 5, 13, 23]). In other parameter regimes, such as high traffic density, this solution is unstable. This is also known from experiments (see [2]).

So far, the dynamics beyond the stable region of the quasi-stationary

state has been an interesting and still widely open question. In [15] a delay differential optimal velocity model was studied in the unstable region. In that case the authors were able to calculate exact multiple solutions and to deduce the existence of bifurcations (subcritical Hopf bifurcations) assuming the special optimal velocity function proposed in [2]. In [15] the same features were mentioned for the standard (non-delay) optimal velocity function models which is studied here in this paper. In [15] we find the conjecture: “our results should be considered to be a universal feature of optimal velocity models”.

In [8] we analyzed the complete dynamics for the standard optimal velocity models with general optimal velocity functions satisfying a few basic properties. In this case no explicit solutions can be calculated. We showed with mathematical rigor that the loss of stability of the quasi-stationary solution is, for general optimal velocity functions, due to a (not necessarily subcritical) Hopf bifurcation. Also we formulated explicitly an analytical criterion concerning the sub- or supercriticality of the Hopf bifurcation. Moreover we studied numerically the global dynamics of the model and its global bifurcation diagram using special continuation codes. We see that the stability condition induced by the linear stability analysis is in general not the relevant condition. Even before the quasi-stationary solution becomes unstable, stable periodic solutions may already (co-)exist (compare with [15]). These solutions correspond to congested traffic situations. Our analysis shows that even simple optimal velocity models have already a rich solution structure with a lot of dynamics. Finally we analyzed the loss of stability of the corresponding quasi-stationary solutions in optimal velocity models with non-equal drivers. There we were able to prove that, in general optimal velocity models, faster (slower) reacting drivers don’t necessarily stabilize (destabilize) traffic. This is in line with the results obtained in [23] concerning the behavior on a circular road. We should mention that on non-circular roads similar phenomena may appear (see [23, 24]). However these are often caused by boundary conditions which have to be imposed in that setting.

In [9] we investigated an extension of the simple optimal velocity model in [8] in two directions: on one hand we considered non-constant reaction times and on the other we included aggressive behavior.

The main issue here is to study the influence of these two extensions on the dynamics. Most of the results can be adapted for this more complex model and once again one can show that the loss of stability of the stationary solution is due to a Hopf bifurcation of which the first Lyapunov coefficient can be explicitly calculated.

At this point we should mention that similar bifurcation phenomena occur in related microscopic traffic flow models. In [14] a model for a bus route

is considered and stability and bifurcation questions are studied. In [26] a bifurcation analysis of a model with delay for cars on a circular road is analyzed.

In the following section I will introduce the general model describing the meaning of its component and making some remarks. To go deeper in the analysis of it, though I will have to relax the generality in different ways and this leads to the simplified models considered in detail in chapters 2 and 3.

1.1 Setting of the problem

Consider a system of N cars moving counterclockwise on a ring of given length \tilde{L} . Fix any origin on the ring and specify the position of each car with a coordinate $\tilde{\theta}$ (\tilde{x} denoting throughout the article that the quantity x has a dimension) and label the cars counterclockwise starting from a random one, so that $\tilde{\theta}_j = \tilde{\theta}_j(\tilde{t})$, $j = 1, \dots, N$ is the coordinate of the j -th car with respect to the chosen origin as a function of time. Let the motion of the cars be described by the following system of ordinary differential equations:

$$\ddot{\tilde{\theta}}_j = \frac{1}{\tilde{T}_j}(\tilde{\theta}_{j+1} - \tilde{\theta}_j) \left\{ \tilde{V}_j(\tilde{\theta}_{j+1} - \tilde{\theta}_j) - \dot{\tilde{\theta}}_j + \alpha_j(\dot{\tilde{\theta}}_{j+1} - \dot{\tilde{\theta}}_j) \tilde{F}_j(\tilde{\theta}_{j+1} - \tilde{\theta}_j) \right\} \quad (1.1)$$

where $j = 1, \dots, N$, $\tilde{\theta}_{N+1} := \tilde{\theta}_1 + \tilde{L}$, α_j are positive constants and the functions $\tilde{V}_j(x)$, $\tilde{T}_j(x)$ and \tilde{F}_j are non-negative and are defined for $x \in \mathbb{R}_+$. Note that these functions might in general depend on one or more parameters.

This is a general follow-the-leader model, appearing often in literature with different specifications for the functions \tilde{V}_j , $\tilde{T}_j(x)$ and \tilde{F}_j , see for example [6, 12, 23, 24]. For a related approach involving delay differential equations, see [15].

Turning to the undimensional (tilde-less) quantities

$$x_j = \frac{\tilde{\theta}_j}{\tilde{a}}, \quad V_j(x) = \frac{\tilde{\tau}}{\tilde{a}} \tilde{V}_j(\tilde{a}x), \quad T_j(x) = \frac{1}{\tilde{\tau}} \tilde{T}_j(\tilde{a}x), \quad t = \frac{\tilde{t}}{\tilde{\tau}}, \quad L = \frac{\tilde{L}}{\tilde{a}}, \quad (1.2)$$

where $j = 1, \dots, N$, \tilde{a} is a characteristic length and $\tilde{\tau}$ is a characteristic time. Introducing variables $y_j = \dot{x}_j$, system (3.1) can be rewritten as

$$\begin{cases} \dot{x}_j = y_j \\ \dot{y}_j = \frac{1}{T_j(x_{j+1} - x_j)} [V_j(x_{j+1} - x_j) - y_j + \alpha_j(y_{j+1} - y_j) F_j(x_{j+1} - x_j)] \end{cases} \quad (1.3)$$

where $j = 1, \dots, N$ and $x_{N+1} := x_1 + L$.

The functions T_j , appearing in (1.3), have the meaning of reaction times for each one of the car-drivers. Their dependence on the headway should enable to mimic the fact that in a denser traffic situation drivers tend to be more alert and react faster than they do when in a relatively empty road. Accordingly the T_j 's should be positively valued functions which monotonically increase with the headway and eventually saturate to a reaction time value of minimal alert.

Aside from the reaction time, the acceleration in system (3.1) is composed of two parts, describing two different but possibly coexisting driving behaviors. The first two terms correspond to the usual law prescribed in car following traffic models (see for example [4, 8, 12, 15, 23]). It states that car j tries to match its velocity to an optimal velocity given by function V_j in terms of the headway. Each one of the V_j 's (V for brevity) will be taken such that it is positively valued and monotonically increasing with its argument, $V(0) = 0$, $\lim_{x \rightarrow \infty} V(x) = V_{max}$ (const.) and $V(x)$ is S-shaped, i.e., there exists a positive constant b such that $V''(x) > 0$ (< 0) if $x < b$ ($> b$). Qualitatively different optimal velocity functions are involved in the case of car-bus systems (see [14]) or in the case of multi-lane traffic (see [16]).

The third term on the right hand side of (1.3) describes a more *aggressive* driving behavior, in that cars try to match the velocity of the car ahead of them. This tendency has been empirically observed and its definitely more marked when cars are driving near to each other, while, when headways grow, drivers tend to care less for what other drivers are doing. Functions F_j are thus taken to be positive defined and decreasing in the headway. The coefficients $\alpha_j \in [0, \infty)$ are *switches*, allowing to choose how much *aggressiveness* driver j has.

As an example, we show two of the OVF's suggested in literature

$$\tilde{V}_L(\tilde{\theta}) = \tilde{V}^{max} \frac{\tilde{\theta}^2}{\tilde{a}^2 + \tilde{\theta}^2}, \quad \tilde{V}_B(\tilde{\theta}) = \tilde{V}^{max} \frac{\tanh\left(\frac{\tilde{\theta}-\tilde{a}}{\tilde{\theta}_0}\right) + \tanh\frac{\tilde{a}}{\tilde{\theta}_0}}{1 + \tanh\frac{\tilde{a}}{\tilde{\theta}_0}} \quad (1.4)$$

Notice that, through the undimensionalization in (1.2), we are actually dealing with the two following functions (see Fig. 1.1)

$$V_L(x) = V^{max} \frac{x^2}{1 + x^2} \quad (\text{solid line}) \quad (1.5)$$

$$V_B(x) = V^{max} \frac{\tanh(a(x-1)) + \tanh(a)}{1 + \tanh(a)} \quad (\text{dashed line}) \quad (1.6)$$

where $V^{max} := \tilde{V}^{max} \tilde{\tau}_{min} / \tilde{a}$ and $a := \tilde{a} / \tilde{\theta}_0$.

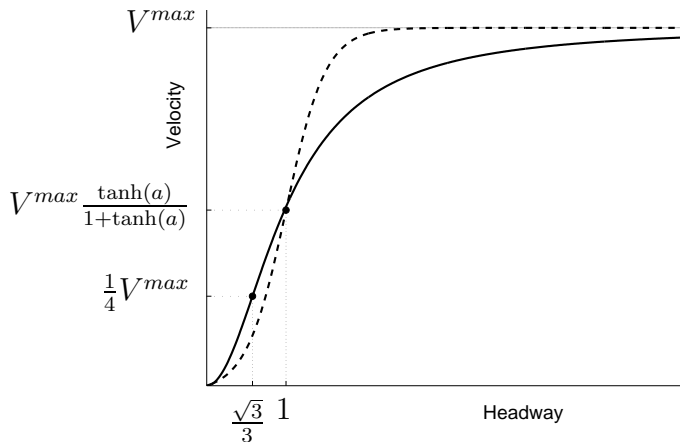


Figure 1.1: Two examples of possible V -functions.

As in the second example, the OVF can depend on more than one (dimensionless) parameter.

The reaction time functions T can be chosen in the same class of functions as the OVF's. A typical choice for F is $F_j(x) = b_j/(x + 1)$ for positive constants b_j .

Historically the optimal velocity part of model (1.3) was introduced in [5] while the other part is much older and goes back to the fifties ([10]).

A further remark about system (1.3) is that it is unable to deal with car-crashes and overtakings in a reasonable way. This means that headways $x_{j+1} - x_j$ can become negative without warning. When this happens, the dynamics doesn't reflect the new ordering of the cars and it is clear that the real world situation is not properly described any more. Moreover one cannot exclude the presence of solutions for which the velocities become negative. We call such solutions as *unphysical*. In the following, alongside the stability of solutions, we have to deal with their physicality too. Note though that we don't regard unphysical solutions as a failure of the model, we just have to be aware of their presence. An interesting approach to be found in literature is that of finding appropriate conditions on the initial data so as to prevent unphysical results (see for ex. [10])

As it is, model (1.3) is hard to deal with so in the following I will study some simplified versions of it.

The second chapter is a treatment of the simplest case where there is no aggressive behavior ($\alpha_j = 0 \forall j$) and the reaction times are constant ($T_j(x) = \tau_j \forall j$). This is then the pure optimal velocity model

In the third chapter I will allow for aggressive behavior and non constant reaction times but this time only in the case where all drivers obey the same

law of motion, i.e. I will drop the dependence on j of OVF's V_j , of the reaction time functions T_j and of the term $\alpha_j F_j$.

Let me underline once more that this material is the result of the work done together with I. Gasser, T. Seidel and B. Werner and it already appeared in the two publications [8, 9].

Chapter 2

Optimal velocity model

I will study here system (1.3) under the assumption that there is no aggressive behavior and that the reaction times are constant, i.e. I set $\alpha_j = 0$ and $T_j(x) = \tau_j$ for all j and x and deal with the simpler system

$$\begin{cases} \dot{x}_j = y_j \\ \dot{y}_j = \frac{1}{\tau_j} [V_j(x_{j+1} - x_j) - y_j] \end{cases} \quad (2.1)$$

The contents of this chapter are a joined work together with I. Gasser and B. Werner and were published in [8].

2.1 Linear analysis

We start looking for special solutions of system (2.1). The following lemma, proved in [23], guarantees existence and uniqueness of a *quasi-stationary* solution (see Remark 2).

Lemma 1 *There is a unique solution $x_j^*(t)$ of (2.1) with constant velocity c for all the cars.*

Remark 1 *Observe that velocity c is not a further independent parameter but it actually depends on L and N .*

Remark 2 *We call solution $x_j^*(t)$ in Lemma 1 quasi-stationary, since the corresponding headways $d_1(c), \dots, d_N(c)$ are constant in time.*

Now setting $x_j(t) = x_j^*(t) + X_j(t)$ and $y_j(t) = c + Y_j(t)$ in system (1.3), leads to

$$\begin{cases} \dot{X}_j = Y_j \\ \dot{Y}_j = \frac{1}{\tau_j} [V_j(d_j(c) + X_{j+1} - X_j) - c - Y_j] \end{cases} \quad j = 1, \dots, N \quad (2.2)$$

where $X_{N+1} = X_1$. Introducing $\mathbf{W} = (\mathbf{X}, \mathbf{Y})$, our quasi-stationary solution $x_j^*(t)$ for system (1.3) is now associated with the equilibrium point $\mathbf{W} = \mathbf{0}$ for (2.2). Linearization around this fixed point leads to the system

$$\dot{\mathbf{W}} = \mathbf{M}\mathbf{W}, \quad \mathbf{M} = \left(\begin{array}{c|c} \mathbf{O}_N & \mathbf{I}_N \\ \mathbf{D}_N & -\mathbf{C}_N \end{array} \right) \quad (2.3)$$

where \mathbf{I}_N is the $(N \times N)$ -identity matrix, \mathbf{O}_N is the $(N \times N)$ -null matrix, \mathbf{D}_N is the matrix

$$\mathbf{D}_N = \begin{pmatrix} -\bar{\beta}_1 & \bar{\beta}_1 & 0 & \dots & 0 \\ 0 & -\bar{\beta}_2 & \bar{\beta}_2 & \ddots & \vdots \\ \vdots & \ddots & \ddots & \ddots & 0 \\ 0 & \dots & 0 & -\bar{\beta}_{N-1} & \bar{\beta}_{N-1} \\ \bar{\beta}_N & 0 & \dots & 0 & -\bar{\beta}_N \end{pmatrix} \quad (2.4)$$

where $\bar{\beta}_j = \frac{1}{\tau_j} V_j'(d_j)$ for $j = 1, \dots, N$ and $\mathbf{C}_N = \text{diag}(1/\tau_1, \dots, 1/\tau_N)$

As already shown in [23], the eigenvalues of \mathbf{M} are the solutions λ of the equation

$$\prod_{j=1}^N (\tau_j \lambda^2 + \lambda + \beta_j) - \prod_{j=1}^N \beta_j = 0, \quad (2.5)$$

where $\beta_j = \tau_j \bar{\beta}_j = V_j'(d_j) \forall j$. Equation (2.5) is too complicated to allow a straightforward analytical insight into the stability of the considered equilibrium point.

The following section deals with the situation where all drivers are equal with respect to V_j and τ_j , which simplifies (2.5). In section 2.4 we then face (2.5) using perturbation arguments to gain insight in the case of individual drivers.

2.2 Drivers with the same driving law: Hopf bifurcation

The most drastic approximation that can be done to system (2.1) (and consequently to system (2.2) and equation (2.5)) is that of imposing that all

drivers should have the same reaction time τ and the same optimal velocity function, i.e. to set $\tau_j = 1$, $V_j(x) = V(x) \quad \forall j$. Under these conditions the quasi-stationary solution of lemma 1 has headways $d_1 = \dots = d_N = L/N$ and velocity $c = V(L/N)$. System (2.2) becomes

$$\begin{cases} \dot{X}_j = Y_j \\ \dot{Y}_j = V\left(\frac{L}{N} + X_{j+1} - X_j\right) - V\left(\frac{L}{N}\right) - Y_j \end{cases} \quad j = 1, \dots, N \quad (2.6)$$

where $X_{N+1} = X_1$, and equation (3.5) is simplified to

$$(\lambda^2 + \lambda + \beta)^N - \beta^N = 0 \quad (2.7)$$

with $\beta = V'\left(\frac{L}{N}\right)$.

The goal is that of studying the influence of the parameter L , the length of the circuit, and with this of the density N/L on the nonlinear system (2.6). We will analyze the (loss of) stability of the trivial equilibrium (or equivalently of the quasi-stationary solution) due to the variation of L for a given number of cars N . To this end we investigate in sec. 2.2.1 how the eigenvalues λ of \mathbf{M} vary with L according to (2.7). Since the parameter L enters \mathbf{M} only via $\beta := V'(L/N)$, we study the dependence of the eigenvalues on β .

We will show that under certain conditions on V , Hopf bifurcations take place for L equal to certain critical lengths L^H . As a consequence periodic solutions of (2.6) exist in a neighborhood of the equilibrium. The critical lengths L^H (and densities $\rho_H = N/L^H$) for which Hopf bifurcations occur, depend on N and certain parameters which enter V as well. This dependence will be also investigated.

To apply the Hopf Theorem (see for example [19]), we have to show that there is a smooth family of eigenvalues $\lambda_{\pm}(L) = \mu(L) \pm i\omega(L)$ of M such that the following conditions are fulfilled:

1. $\mu(L^H) = 0$, i.e. for the critical parameter L^H there is a pair $\pm i\omega(L^H)$ of purely imaginary eigenvalues of the matrix M .
2. There are no other eigenvalues of M on the imaginary axis for $L = L^H$.
3. Eigenvalue-crossing condition: $\mu'(L^H) \neq 0$.
4. The first Lyapunov coefficient ℓ does not vanish.

The last condition is a non-degeneracy condition which allows a conclusion about the stability of the bifurcating periodic solutions if the first

condition is sharpened requiring all other eigenvalues of M for $L = L^H$ to be located in the left half complex plane.

We remark that $\lambda = 0$ is always an eigenvalue of M for all parameters. This contradicts the second Hopf condition. But we will show in sec. 2.2.2 that this eigenvalue can be eliminated due to a rotational symmetry in the system.

2.2.1 Structure of the eigenvalues

Setting $\lambda = \mu + i\omega$, equation (2.7) is equivalent to

$$\begin{cases} \mu^2 - \omega^2 + \mu = \beta(c_k - 1) \\ \omega(2\mu + 1) = \beta s_k \end{cases} \quad k \in \{1, \dots, N\} \quad (2.8)$$

where $c_k = \cos(2\pi k/N)$ and $s_k = \sin(2\pi k/N)$. Notice that for $k = N$ the points $(\mu, \omega) = (0, 0)$ and $(\mu, \omega) = (-1, 0)$ are solutions of the system for every β . The reason for this will become clear in sec. 2.2.2, where the $2N$ -system is reduced to a $(2N - 2)$ -system where these two eigenvalues don't appear anymore but all the other eigenvalues remain unchanged.

For every fixed N and $k \neq N$, system (2.8) is the parametric representation of two hyperbolically shaped branches with regard to the parameter $\beta > 0$, as shown in Fig.2.1 for $N = 5$.

The whole set of eigenvalues has a central symmetry with respect to the point $C = (-\frac{1}{2}, 0)$. For $\beta = 0$, N eigenvalues are located in the origin O and N in the point $S = (-1, 0)$. As soon as β grows, the two eigenvalues associated with $k = N$ stay in S and in O respectively, while all the other eigenvalues separate from each other flowing along the hyperbolic branches, as represented by the arrows on the curves. For sufficiently small $\beta > 0$, all the eigenvalues lie in the left complex plane, which implies the asymptotic stability of our quasi-stationary solution. As β is increased more and more, a pair of complex conjugate eigenvalues might cross the imaginary y -axis causing loss of stability. The 'right' k -th branch intersects the y axis at the same time as the 'right' $(N - k)$ -th branch, and this happens when the following relation is satisfied

$$\beta = \beta_k := \frac{1 - c_k}{s_k^2} = \frac{1}{1 + c_k}, \quad (2.9)$$

the above being valid for $k = 1, 2, \dots, N'$, where $N' := \lfloor (N-1)/2 \rfloor$. Note that in the limit for large N , crossing relation (2.9) reduces to $\beta = 1/2$ independently of k . This is the usual instability threshold given in literature (see for example [5, 23]).

It is easily checked that the couple of eigenvalues which intersects the imaginary axis for the lowest value of β , corresponds to $k = 1$ (and to $k = N - 1$), followed for increasing values of β by the one corresponding to $k = 2$ (and to $k = N - 2$) and so on.

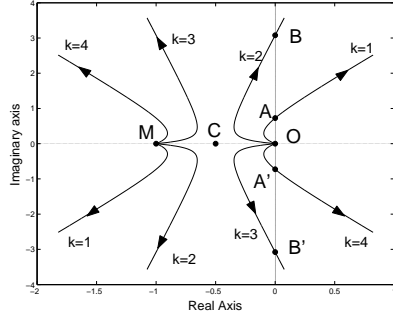


Fig. 2.1: Eigenvalues for five cars ($N = 5$).

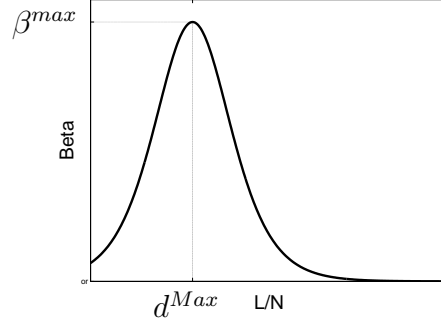


Fig. 2.2: β as a function of L/N and fixed a

Therefore, as far as the stability of the quasi-periodic solution is concerned, only the case where the first two eigenvalues cross the imaginary axis for $\beta = \beta_1$ is relevant. For the corresponding branch of eigenvalue pairs $\lambda(\beta) = \mu(\beta) \pm i\omega(\beta)$ we have the following:

Lemma 2

$$\omega(\beta_1) = s_1\beta_1, \quad \mu'(\beta_1) = \frac{s_1^2}{5 - 3c_1}, \quad (2.10)$$

For a proof one has to differentiate system (2.8) with respect to β .

Lemma 2 is an eigenvalue crossing condition which appears in the Hopf Theorem. But observe that not β , but L is the parameter in (2.6). To this purpose we have to solve $V'(L/N) = \beta$ for L , and the Hopf conditions have to be checked in terms of the eigenvalues $\tilde{\lambda}(L) := \mu(V'(L/N)) \pm i\omega(V'(L/N))$. The critical β_1 corresponds to critical lengths L^H given by

$$V'(L^H/N) = \beta_1 = \frac{1}{1 + c_1}. \quad (2.11)$$

This is where the graph of V' enters the game, see Fig. 2.2. From the assumptions on V follows that $V'(x)$ is bell-shaped. Let β^{max} be the maximum of $V'(x)$ and $\beta^{max} = V'(d^{max})$. If $\beta_1 > \beta^{max}$, there is no solution of (2.11) – the equilibrium is stable for all L , no bifurcations at all, see Fig. 2.3(a). The case $\beta_1 = \beta^{max}$ leads to a degenerated Hopf point – we will not consider this case. Instead we assume from now on that $\beta_1 < \beta^{max}$. Then there exist two

solutions L_-, L_+ of (2.11) satisfying $L_- < d^{max} < L_+$. The corresponding critical densities are $\rho_- := N/L_-$ and $\rho_+ := N/L_+$. The eigenvalue crossing condition remains valid, since $V''(L/N) \neq 0$ for $L = L_{\pm}$. Disregarding the eigenvalue $\lambda = 0$, $\pm\omega_1$ are the only eigenvalues of M on the imaginary axis for $L = L^H$. Hence the Hopf conditions are fulfilled for $L^H = L_{\pm}$, only the last condition concerning the Lyapunov coefficient has to be analyzed.

It might be helpful to visualize how the complex conjugate eigenvalue pairs $\tilde{\lambda}(L)$ of M behave when L is varied. To this end we start with rather large L (and small densities) for which $V'(L/N) < \beta_1$. All eigenvalues of M have negative real part (excepted the zero-eigenvalue). Decreasing L (and increasing the density) down to $L = L_+$ results in a pair of purely imaginary eigenvalues of M which crosses the imaginary axis when L is further decreased. If $V'(L/N) = \beta^{max}$ (for $L/N = d^{max}$), the real parts of the eigenvalues are maximal, further eigenvalues numbered by $k = 2, 3, \dots$ have crossed the imaginary axis if $\beta_k < \beta^{max}$, see Fig. 2.3(c). If $\beta_2 > \beta^{max}$, no further eigenvalues have entered the right complex half plane, see Fig. 2.3(b). A further decrease of L leads to a turning back of all eigenvalues in the right half of the complex plane. For $L = L_-$ the last of these eigenvalue curves cross the imaginary axis with nonzero speed at the same locus where it entered the right half of the complex plane leading to a second Hopf bifurcation with the same β_1 . The trivial equilibrium (and hence our quasi-stationary solution) becomes stable again, while it is unstable for all $L \in (L_-, L_+)$.

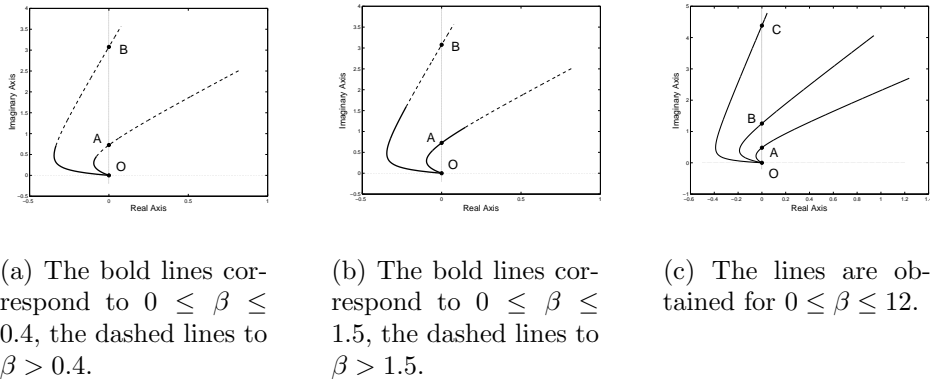


Figure 2.3: Three qualitatively different scenarios for the behavior of the eigenvalues. The first two pictures are obtained for $N = 5$ and the third for $N = 7$.

It is not unimportant to investigate the dependence of the critical β_1 in

(2.11) (and L_{\pm}) on the number of cars N – the dimension of our nonlinear system (2.6). While $c_1 = 1 - O(1/N^2)$ increases with N , the parameter β_1 decreases with N , we have $\beta_1 = 0.5 + O(1/N^2)$. Hence the condition $\beta_1 < \beta^{max}$ is always fulfilled for sufficiently large N if $0.5 < \beta^{max}$. Concerning the critical lengths, L_-/N decreases, while L_+/N increases slightly with increasing N . Asymptotically, taking the two solutions $x_-^0 < x_+^0$ of $\tilde{V}(x) = 0.5$ we obtain $L_-/N = x_-^0 + O(1/N^2)$ and $L_+/N = x_+^0 - O(1/N^2)$. Since $c_1 \approx 1$ for for already not too large N , there are essentially two different critical densities $\rho_+ := 1/x_-^0$ and $\rho_- := 1/x_+^0$ for sufficiently (moderately) large N . For densities $\rho = N/L$ with $\rho_- < \rho < \rho_+$ we expect – at least for sufficiently large N – unstable quasi-stationary solutions which are either stabilized by decreasing the density to $\rho < \rho_-$ or by increasing it to $\rho > \rho_+$.

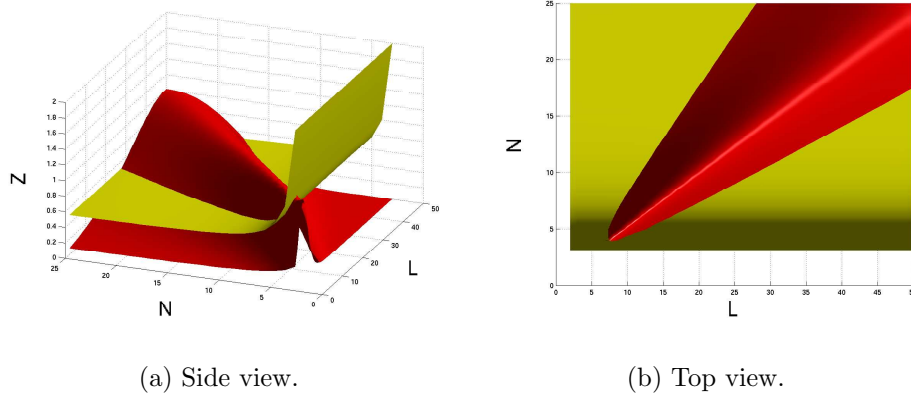


Figure 2.4: In red surface $Z(L, N) = V'(\frac{L}{N})$, in yellow surface $Z(L, N) = \frac{1}{1+c_1} = (1 + \cos \frac{2\pi}{N})^{-1}$.

Fig.2.4(a) is a 3-dimensional representation. The red surface is the graph of $Z(L, N) = V'(\frac{L}{N})$, while the yellow surface is the graph of $Z(L, N) = \frac{1}{1+c_1} = (1 + \cos \frac{2\pi}{N})^{-1}$. The intersection of these two surfaces corresponds to the points that verify the Hopf relation (2.11)

Fig.2.4(b), which is a top view of Fig.2.4(a), shows in red the (instability) region of the (L, N) -plane in which the first couple of eigenvalues has positive real part. Note that the Hopf curve given by points (L, N) satisfying (2.11) is just the common border of the red and the yellow region. For larger N , it consists of two straight lines due to our asymptotics above.

Notice that, though we have been talking about surfaces for clarity, one can correctly do so only *pretending* that N is a continuous variable, while of

course it isn't.

2.2.2 Bifurcation analysis

We have already checked three of the four conditions of the Hopf theorem, showing that (2.6) undergoes a Hopf bifurcation for critical lengths L_{\pm} , if we disregard the eigenvalue $\lambda = 0$. The main task is the computation of the Lyapunov coefficient ℓ .

The main result of this paper reads as follows

Theorem 1 *Let be*

$$\beta_1 = \frac{1}{1 + \cos \frac{2\pi}{N}} < \beta^{max} := \max_x V'(x).$$

Then system (2.6) undergoes a Hopf bifurcation for the two critical lengths L_{\pm} which are the two solutions of $V'(L/N) = \beta_1$.

The two corresponding first Lyapunov coefficients are

$$\ell_{\pm} = \frac{s_1(c_1 + 1)}{2(5 - 3c_1)} \left[V''' \left(\frac{L_{\pm}}{N} \right) - \frac{(V''(\frac{L_{\pm}}{N}))^2}{V'(\frac{L_{\pm}}{N})} \right] \quad (2.12)$$

where $s_1 = \sin \frac{2\pi}{N}$ and $c_1 = \cos \frac{2\pi}{N}$. Moreover, if $\ell < 0$ (> 0), the bifurcation is supercritical (subcritical).

Remark 3 *This means that in the case $\ell < 0$ (> 0) we have locally stable (unstable) periodic solutions.*

Remark 4 *The above theorem is valid for any positively valued, monotonically increasing and bounded OVF.*

Sketch of proof and remarks: We want to apply the Hopf theorem to system (2.6), but unfortunately this can't be done directly because the matrix \mathbf{M} , appearing in the linearized version of this system, is singular. We can solve this problem introducing the variables $\phi_j = X_{j+1} - X_j + L/N$ (headways) and $\eta_j = Y_{j+1} - Y_j$ (relative velocities). The occurrence of the zero eigenvalue is due to the conserved quantity $\sum_{j=1}^N \phi_j = L$. Using this relation together with $\sum_{j=1}^N \eta_j = 0$, we can eliminate variables x_N and y_N and rewrite system (2.6) as

$$\begin{cases} \dot{\phi}_i = \eta_i & i = 1, \dots, n \\ \dot{\eta}_i = V(\phi_{i+1}) - V(\phi_i) - \eta_i & i = 1, \dots, n-1 \\ \dot{\eta}_n = V(L - \sum_{k=1}^n \phi_k) - V(\phi_n) - \eta_n \end{cases} \quad (2.13)$$

with $n = N - 1$, or, writing $\mathbf{w} = (\phi, \eta)$

$$\dot{\mathbf{w}} = \mathbf{G}(\mathbf{w}), \quad \mathbf{w} \in \mathbb{R}^{2n} \quad (2.14)$$

If we express system (2.14) in the form

$$\dot{\mathbf{w}} = \mathbf{A}\mathbf{w} + \mathbf{g}(\mathbf{w}), \quad \mathbf{g}(\mathbf{w}) = \mathbf{0}(\|\mathbf{w}\|^2) \quad (2.15)$$

then matrix \mathbf{A} is regular and has the same eigenvalues of matrix \mathbf{M} except 0 and -1 . It has the block structure

$$\mathbf{A} = \left(\begin{array}{c|c} \mathbf{O}_n & \mathbf{I}_n \\ \hline \mathbf{B}_n(\beta) & -\mathbf{I}_n \end{array} \right) \quad (2.16)$$

with

$$\mathbf{B}_n(\beta) = \begin{pmatrix} -\beta & \beta & 0 & \dots & \dots & 0 \\ 0 & -\beta & \beta & \ddots & \ddots & \vdots \\ \vdots & \ddots & \ddots & \ddots & \ddots & \vdots \\ \vdots & \ddots & \ddots & \ddots & \ddots & 0 \\ 0 & \dots & \dots & 0 & -\beta & \beta \\ -\beta & \dots & \dots & \dots & -\beta & -2\beta \end{pmatrix} \quad (2.17)$$

Note that the parameter L doesn't appear anymore, but \mathbf{A} depends on it via $\beta = V'(L/N)$ and the nonlinearity $\mathbf{g}(\mathbf{w})$ depend on L . Next we need some formula to calculate the quantity ℓ_{\pm} for $L = L_{\pm}$. Set $\lambda(\beta_1) = \lambda_{\pm} = \pm i\omega_1$ with $\omega_1 > 0$ and let $\mathbf{q}, \mathbf{p} \in \mathbb{C}^n$ be respectively an eigenvector corresponding to λ_+ and its adjoint, satisfying the normalization $\langle \mathbf{p}, \mathbf{q} \rangle = 1$ (the standard scalar product in \mathbb{C}^n is taken to be anti-linear in the first argument). Consider also the two multilinear functionals $\mathbf{B}(\mathbf{x}, \mathbf{y})$ and $\mathbf{C}(\mathbf{x}, \mathbf{y}, \mathbf{z})$ defined as

$$\begin{aligned} B_i(\mathbf{x}, \mathbf{y}) &= \sum_{j,k=1}^n \frac{\partial^2 G_i(\xi)}{\partial \xi_j \partial \xi_k} \Big|_{\xi=0} x_j y_k \\ C_i(\mathbf{x}, \mathbf{y}, \mathbf{z}) &= \sum_{j,k,l=1}^n \frac{\partial^3 G_i(\xi)}{\partial \xi_j \partial \xi_k \partial \xi_l} \Big|_{\xi=0} x_j y_k z_l \end{aligned} \quad (2.18)$$

where $i = 1, \dots, 2n$. Observe that these multilinear functionals depend on L_{\pm} , while \mathbf{A} and hence both \mathbf{p} and \mathbf{q} are the same for $L = L_-$ and $L = L_+$, since $\beta_1 = V'(L_{\pm}/N)$. Then we have the following invariant expression for the first Lyapunov coefficient (see [19] for a proof of this formula):

$$\begin{aligned} \ell = \frac{1}{2\omega_1} \operatorname{Re} \left[& \langle \mathbf{p}, \mathbf{C}(\mathbf{q}, \mathbf{q}, \bar{\mathbf{q}}) \rangle - 2 \langle \mathbf{p}, \mathbf{B}(\mathbf{q}, \mathbf{A}^{-1}(\beta_1)\mathbf{B}(\mathbf{q}, \bar{\mathbf{q}})) \rangle + \\ & + \langle \mathbf{p}, \mathbf{B}(\bar{\mathbf{q}}, (2i\omega_1\mathbf{I} - \mathbf{A}(\beta_1))^{-1}\mathbf{B}(\mathbf{q}, \mathbf{q})) \rangle \right] \end{aligned} \quad (2.19)$$

A direct calculation leads now to formula (2.12). In the appendix we explicitly calculate ℓ in the more complicated case of non-zero aggressive term and non-constant reaction times.

Remark 5 Notice that for $N > 2$ the quantity $s_1(c_1+1)(5-3c_1)^{-1}$, appearing as a coefficient in (2.12), is positive and, since we are only interested in the sign of ℓ , it is sufficient to study the factor in square brackets which will be referred to as $\hat{\ell}$ in the following.

2.2.3 Discussion for different optimal velocity functions

We analytically proved that system (2.6) undergoes a Hopf bifurcation if L and N are such that

$$V'\left(\frac{L}{N}\right) = \frac{1}{1 + \cos \frac{2\pi}{N}} \quad (2.20)$$

and if the quantity

$$\hat{\ell} = V'''\left(\frac{L}{N}\right) - \frac{(V''(\frac{L}{N}))^2}{V'(\frac{L}{N})} \quad (2.21)$$

related to the first Lyapunov coefficient of the bifurcation, is non-zero. Moreover, the Hopf bifurcation is supercritical if $\hat{\ell} < 0$ and subcritical if $\hat{\ell} > 0$.

As examples, we calculate $\hat{\ell}$ for the two optimal velocity functions mentioned in sec. ???. For $V_B(x)$ as in (1.6) we have

$$\hat{\ell} = -C \left[1 - h\left(\frac{L}{N}\right) \right]^2 \quad (2.22)$$

where C is a positive constant and $h(x) = \tanh^2(a(x-1))$. Then $\hat{\ell}$ is always negative and we conclude that the OVF (1.6) only allows the development of supercritical Hopf bifurcations. Fig.2.5 represents the implicit curve (2.20) in the (N, L) -plane with (1.6) as a V function. Following from top to bottom the vertical line drawn at $N = 12$, we are ideally shrinking the circuit on which our twelve cars are moving. For a certain value of L we encounter

the parabolic-like curve and a supercritical Hopf bifurcation takes place. We are guaranteed by our previous analysis that the fixed point \mathbf{w}_0 becomes unstable and stable periodic orbits are generated in its vicinity. We will see in the next chapter that a numerical analysis shows that this behavior is not only local but extended to all the interval between the two bold points of intersection of the vertical line and the curve. If we continue to decrease L , we reach the second intersection point and the Hopf bifurcation is, once again supercritically, absorbed and the fixed point becomes again the only stable element in the phase space of the system.

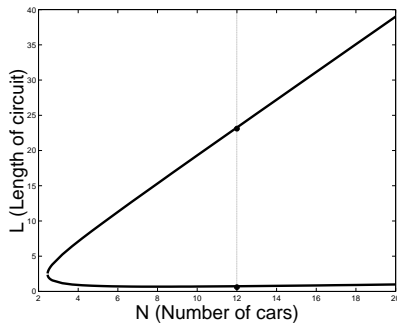


Fig. 2.5: Bifurcation diagram for the hyperbolic optimal velocity function (1.6).

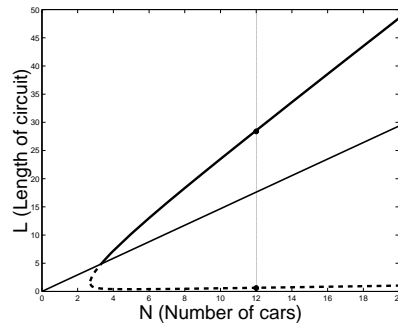


Fig. 2.6: Bifurcation diagram for the logistic optimal velocity function (1.5).

If we now try function (1.5), we obtain

$$\hat{\ell} = C \frac{3d^4 - 6d^2 - 1}{x(1 + d^2)^4} \quad (2.23)$$

where C is a positive constant and $d = \frac{L}{N}$. In this case the quantity $\hat{\ell}$ is null for $d^* = \sqrt{1 + \frac{2}{3}\sqrt{3}} \simeq 1.4679$ and if the critical density defined by (2.20) is less than d^* the transition is supercritical, otherwise it's subcritical. The bifurcation diagram in the (N, L) -plane is this time represented in Fig.2.6, where we also drew the line $L = d^*N$ separating an upper continuous curve of subcritical Hopf bifurcations and a lower dashed curve of supercritical Hopf bifurcations.

Both Fig.2.5 and 2.6 show that, though technically the system undergoes two Hopf bifurcations, the only interesting one is the one taking place for the higher value of L . In fact it can be seen that the other one takes place for a very short circuit and a comparatively large amount of cars, attempting to describe a situation where the hypothesis of point-like cars fails.

2.3 Drivers with the same driving law: numerical bifurcation analysis

In the previous section we presented an exhaustive analytical description of the behavior of the system in the proximity of eventual Hopf bifurcation points. These results are though local and do not give us insight into the global stability of the Hopf branches nor do they enable us to detect any further bifurcation that may take place on these branches. We thus use the software AUTO2000 to numerically obtain more detailed bifurcation diagrams for system (2.6).

The following diagrams are relative to the already mentioned optimal velocity function

$$V_B\left(\frac{L}{N}\right) = V^{max} \frac{\tanh\left(a\left(\frac{L}{N} - 1\right)\right) + \tanh(a)}{1 + \tanh(a)} \quad (2.24)$$

This choice means that, according to the discussion in subsection 3.4, all the Hopf bifurcations from the quasi-stationary solution are going to be supercritical.

In section 3 we focused on the case of just one Hopf bifurcation, using then L as a free parameter to investigate the local characteristics of the bifurcation itself. We want now to also allow the case of no bifurcation as well as the case of multiple bifurcations. This can be controlled letting the maximal velocity V^{max} vary alongside with L . On the other hand N is always thought of as fixed, being it not suitable as a bifurcation parameter due to the fact that it is intrinsically discrete and that it controls the dimension of the system itself.

Fig.2.7 is analogous to figures 2.3(a), 2.3(b) and 2.3(c) and it shows how increasing V^{max} increases the maximum of function $V'(\frac{L}{N})$ allowing, as L is varied, for more and more Hopf bifurcations to take place.

Each of the following bifurcation diagrams is calculated for a fixed value of V^{max} , has L on the horizontal axis and a numerical L_2 -norm of the solution on the vertical axis. Moreover the points of continuous curves represent stable solutions (fixed points or orbits) while those on dashed curves are relative to unstable solutions.

The dot-dashed curve in Fig.2.7 corresponds, as L is varied, to a branch of stable fixed points. For each fixed L , we have only one fixed point \mathbf{w}_0 . No periodic solutions bifurcate from it. Figures 3.8 and 2.9 are both related to the situation described by the dashed curve in Fig. 2.7. In Fig. 3.8(a) we witness the birth of a simple supercritical Hopf bifurcation as L is varied. Say we move along the skew branch from right to left (decreasing values of L),

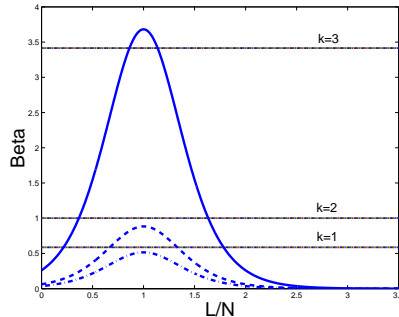
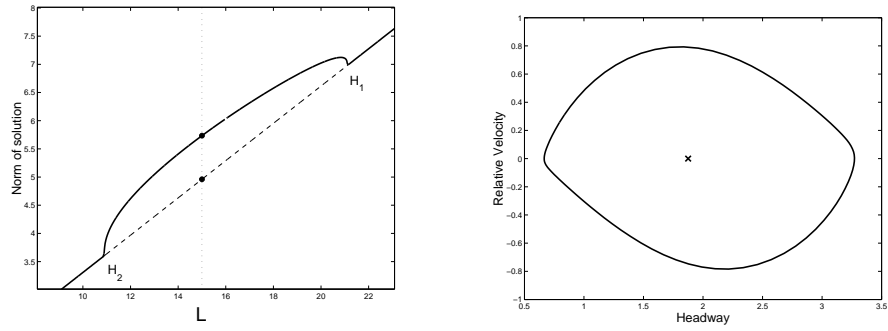


Figure 2.7: Function (2.24) for $N = 8$, $a = 2$ and $V^{max} = 7$ (dot-dashed curve), $V^{max} = 12$ (dashed curve) and $V^{max} = 50$ (continuous curve). The horizontal lines correspond to the quantity $(1 + \cos \frac{2\pi k}{N})^{-1}$ calculated for the indicated values of k .

then we have at first a stable fixed point that eventually loses its stability in favor of a periodic solution which grows in norm and then shrinks again collapsing on the fixed point in the left Hopf bifurcation. After that we are once again left with a stable fixed point. Fig.3.8(b) portrays the solutions represented by the bolt points in diagram 3.8(a) in a slice of the phase space of the system relative to the i -th car, i.e. the plane (x_i, y_i) . We see there the unstable fixed point surrounded by a stable cycle. Note that, due to the rotational group symmetry of system (2.6), Fig.3.8(b) is the same for every car, i.e. for every i .

The situation in Fig.2.9 is similar, but a new effect appears. Four fold bifurcations take place on the Hopf bifurcation branch. The blow-up of the right Hopf bifurcation and the phase portrait of the bold solutions in it (Fig.2.9(b)) show that for an interval of values of L we have an unstable fixed point surrounded by a stable cycle, an unstable cycle and once again a stable cycle. In this case there are two stable objects in the phase space of the system, so that, according to the initial conditions, trajectories will spiral toward one of the two and a sufficiently big perturbation can permanently change the long term behavior of the system.

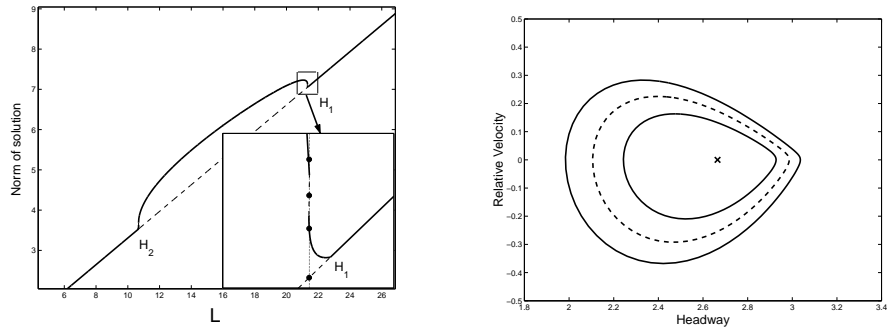
Let's turn now to Fig.2.10. We can see that, as V^{max} is increased, the two folds F_1 and F_2 move outward eventually passing the verticals on the Hopf bifurcations. This is an even bigger qualitative change, because, as shown in Fig.2.10(b), even for a value of L bigger than the analytically forecast critical value, the system can jump to a periodic orbit. Although even the detail in Fig.2.10(a) doesn't allow to observe this, the behavior is locally supercritical but macroscopically subcritical. This should be compared with the subcritical



(a) Two supercritical Hopf bifurcation points joined by a branch of stable periodical solutions.

(b) The two solutions corresponding to the bold dots in Fig.3.8(a) projected on the phase space relative to one car. The cross indicates the unstable fixed point.

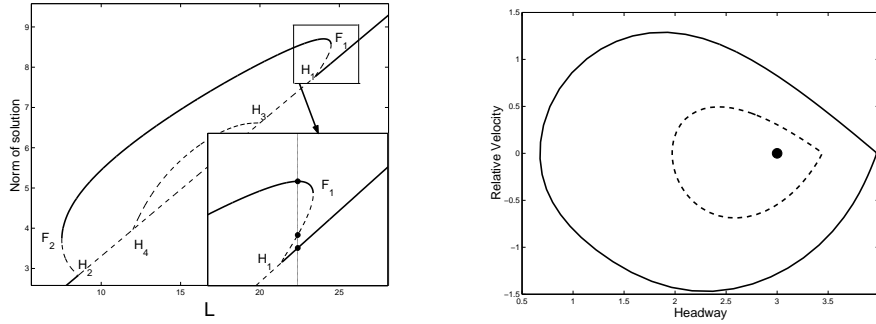
Figure 2.8: Bifurcation diagram and phase space portrait of two solutions for $N = 14$, $a = 2$ and $V^{max} = 34$.



(a) Two supercritical Hopf bifurcation points joined by a branch of periodical solutions. In the blow-up two fold bifurcations can be seen. Between them the orbits are unstable.

(b) Phase space for one car. The dashed orbit is unstable.

Figure 2.9: Bifurcation diagram and phase space portrait of some solutions for $N = 14$, $a = 2$ and $V^{max} = 35$.



(a) The bifurcation in H_1 is locally supercritical but macroscopically subcritical.

(b) Phase space for one car. Bold dotted solutions in Fig.2.10(a). Even before the Hopf point there is a stable periodic orbit surrounding it.

Figure 2.10: Bifurcation diagram and phase space portrait of some solutions for $N = 14$, $a = 2$ and $V^{max} = 50$.

phenomenon shown in [15], note though that the model there involves a delay differential equation, fact that makes a direct comparison impossible. Again Fig.2.10 shows the appearance of a second Hopf bifurcation branch (solid curve in Fig.2.7) which is though of secondary importance since its solutions are unstable cycles. This holds for all the further branches that originate one inside the other as V^{max} is increased (Fig.3.4).

In Fig.2.12 we have a three dimensional bifurcation diagram of the system. Hopf bifurcation surfaces other than the first one are not drawn.

2.4 Perturbative argument for non-equal drivers

We now go back to the general eigenvalue equation (3.5). It is trivial to see that for any eigenvalue λ of (3.5), $\bar{\lambda}$ is an eigenvalue too. Supposing that, for some fixed N -tuple β_1, \dots, β_N , a couple of eigenvalues lies the imaginary axis while all the other eigenvalues have negative real part, we investigate how a small perturbation of the reaction times of the drivers affects the stability of the system. We call $\lambda_H = \pm i\omega$ the couple of eigenvalues with null real part. Writing equation (3.5) for λ_H , we obtain

$$\prod_{j=1}^N (\gamma_j + i\omega) = \prod_{j=1}^N \beta_j \quad (2.25)$$

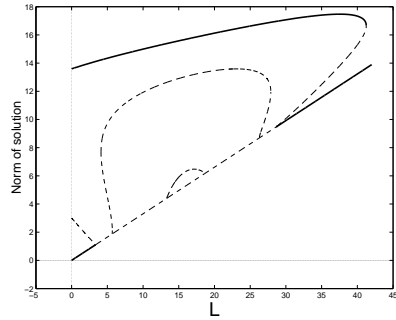


Figure 2.11: Bifurcation diagram and phase space portrait of some solutions for $N = 14$, $a = 2$ and $V^{max} = 150$. All continuation branches connecting couples of Hopf bifurcation points other than the first one are composed of unstable orbits.

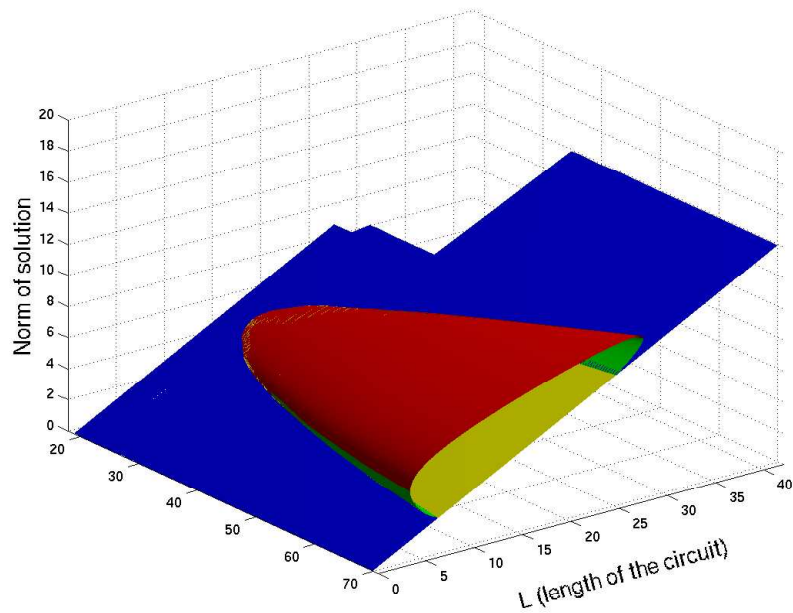


Figure 2.12: 3D bifurcation diagram. Free parameter are L and V^{max} . In blue stable fixed points, in yellow unstable fixed points, in red stable periodical solutions, in green unstable periodical solutions.

where $\gamma_j = \beta_j - \tau_j \omega^2$. Now perturb the τ_j assuming that

$$\alpha_i = \tau_i + \epsilon A_i, \quad i = 1, \dots, N \quad (2.26)$$

where $\epsilon > 0$ is a small parameter. Then the eigenvalues become

$$\lambda = \lambda(\epsilon), \quad \lambda(0) = \lambda_H. \quad (2.27)$$

Substituting (2.26) into (3.5) and differentiating with respect to ϵ leads to

$$\lambda'(0) \sum_{j=1}^N \frac{1 + i\delta_j}{\gamma_j + i\omega} = \omega^2 \sum_{j=1}^N \frac{A_j}{\gamma_j + i\omega} \quad (2.28)$$

where $\delta_j = -2\omega\tau_j$.

We can now state the following lemmas, dealing respectively with the case of weakly individual drivers and with the case of two co-existing types of vehicles.

Lemma 3 *Suppose all drivers have equal reaction times τ and optimal velocity function V . Then small disturbances of the form (2.26) of the scaled reaction times stabilize (destabilize) the “stationary” solution if*

$$\sum_{i=1}^N A_i < 0 \quad (> 0). \quad (2.29)$$

PROOF : Setting $\tau_j = \tau$ and $\beta_j = \beta \quad \forall j$ in (2.28), we get

$$Re \lambda'(0) = \frac{\omega^2}{N(1 + 4\omega^2\tau^2)} \sum_{j=1}^N A_j \quad (2.30)$$

q.e.d.

Consider now the case of $N - m$ drivers with reaction time τ and m drivers with different reaction time, say $\hat{\tau}$. All drivers have the same β (same optimal velocity function) but a part of them reacts sensibly slower or faster than the other one. We could think of a mixed traffic flow situation with cars and trucks driving on the same street. Since equation (2.25) (and with it the bifurcational behavior of the system) does not depend on the sequence in which the vehicles travel on the road, we are free to consider the first m vehicles as being the elements of the first type (say the trucks) and the following $N - m$ as all those of the second type (the cars). The perturbations described by (2.26) become here

$$\tau_i + \epsilon A_i = \begin{cases} \hat{\tau} + \epsilon A_i & i = 1, \dots, m \\ \tau + \epsilon A_i & j = m + 1, \dots, N \end{cases} \quad (2.31)$$

Call

$$\begin{aligned} \delta = -2\omega\tau, \quad \hat{\delta} = -2\omega\hat{\tau}, \quad \gamma = \beta - \omega^2\tau, \quad \hat{\gamma} = \beta - \omega^2\hat{\tau} \\ \hat{A} = \sum_{j=1}^m A_j, \quad A = \sum_{j=m+1}^N A_j \end{aligned} \quad (2.32)$$

Lemma 4 *In the case of two types of vehicles, a decrease of the reaction times stabilizes (destabilizes) the "stationary" solution if and only if*

$$|\omega^2(\tau - \hat{\tau}) - \Sigma| < \Gamma \quad (> \Gamma) \quad (2.33)$$

where

$$\Sigma = \frac{m(\beta + \omega^2\hat{\tau})A - (N - m)(\beta + \omega^2\tau)\hat{A}}{2[mA + (N - m)\hat{A}]} \quad (2.34)$$

$$\Gamma = \sqrt{\Sigma^2 + \frac{m(\gamma^2 + \omega^2) + (N - m)(\hat{\gamma}^2 + \omega^2)}{mA + (N - m)\hat{A}}(A + \hat{A})} \quad (2.35)$$

PROOF With the hypotheses of the lemma we have $A \geq 0$ and $\hat{A} \geq 0$, while equation (2.28) becomes

$$\lambda'(0) \left[(N - m) \frac{1 + i\delta}{\gamma + i\omega} + m \frac{1 + i\hat{\delta}}{\hat{\gamma} + i\omega} \right] = \omega^2 \left[\frac{A}{\gamma + i\omega} + \frac{\hat{A}}{\hat{\gamma} + i\omega} \right] \quad (2.36)$$

a direct calculation shows that $Re[\lambda'(0)] = C(\xi - \xi_+)(\xi - \xi_-)$, where C is a positive quantity, $\xi = \omega^2(\hat{\tau} - \tau)$ and $\xi_{\pm} = \Sigma \pm \Gamma$. Now (2.33) immediately follows. *q.e.d.*

This result shows that, if the reaction times of the two populations are very different from each other, a decrease of the reaction times does not necessarily imply a stabilizing effect as in case of similar reaction times tackled in the previous result. We see that decreasing the reaction times of one type of vehicles stabilizes the traffic provided that the ratio between its own number of elements and the number of the vehicles of the other kind is big enough. However, for a fixed number of vehicles on a circular road this ratio is bounded from above (as long as we don't eliminate one type of vehicles)

and may not reach the required stabilizing limit. Therefore when more than one type of vehicles are present, we expect dynamical effects which are not known in the case of equal cars. These results go in the same direction as [23]. However, in [23] the stability is studied depending on the ratio of the numerosity of the two vehicle groups. Here we study the influence of changing the reaction times under appropriate conditions.

Chapter 3

Aggressive drivers and variable reaction times

In this chapter I will consider the case of drivers obeying the same driving law but with aggressive behavior and reaction times dependent on the headway. Under these conditions system (1.3) is equivalent to the following law of motion for the cars

$$\ddot{x}_j = \frac{1}{T(x_{j+1} - x_j)} \left\{ V(x_{j+1} - x_j) - \dot{x}_j + \alpha \cdot (\dot{x}_{j+1} - \dot{x}_j) F(x_{j+1} - x_j) \right\}, \quad (3.1)$$

where $j = 1, \dots, N$ and $x_j(t)$ is the distance of car j from a given origin with the prescription $x_{N+1} := x_1 + L$.

The contents of this chapter have been published in [9] and are the product of a joined work with I. Gasser, T. Seidel and B. Werner.

3.1 Linear and local bifurcation analysis

It is convenient to rewrite system (3.1) with respect to the variables $\phi_j = x_{j+1} - x_j$ and $\psi_j = \dot{x}_j$ with the prescription $\psi_{N+1} := \psi_1$. We get the system

$$\begin{cases} \dot{\phi}_j = \psi_{j+1} - \psi_j \\ \dot{\psi}_j = \frac{1}{T(\phi_j)} [V(\phi_j) - \psi_j + \alpha \cdot (\psi_{j+1} - \psi_j) F(\phi_j)] \end{cases} \quad (3.2)$$

for $j = 1, \dots, N$. Note that, although we consider relative distances (headways) ϕ_j as variables as in chapter 2, we do not do the same with relative velocities, keeping absolute velocities ψ_j . This actually simplifies matters in the case of non-constant T (compare to [8]).

Because of the assumptions on function V and of the fact that $\sum_{k=1}^N \phi_k = L$, system (3.2) admits as the only stationary solution $\phi_j^s = L/N$, $\psi_j^s = V(L/N)$ for $j = 1, \dots, N$. Introducing variables $\xi_j = \phi_j - L/N$, $\eta_j = \psi_j - V(L/N)$ for $j = 1, \dots, N$ and $\mathbf{w} = (\xi, \eta)$, the stationary solution becomes $\mathbf{w}^s = \mathbf{0}$. Linearizing around $\mathbf{w}^s = \mathbf{0}$ we find a system of the form $\dot{\mathbf{w}} = \mathbf{M}\mathbf{w}$, where the $2N \times 2N$ matrix \mathbf{M} has the structure

$$\mathbf{M} = \left(\begin{array}{c|c} \mathbf{O}_N & \mathbf{D} \\ \hline \frac{\beta}{\tau} \mathbf{I}_N & \frac{\gamma}{\tau} \mathbf{D} - \frac{1}{\tau} \mathbf{I}_N \end{array} \right) \quad (3.3)$$

where $\beta = V'(d)$, $\gamma = \alpha F(d)$, $\tau = T(d)$, \mathbf{I}_N is the $(N \times N)$ -identity matrix, \mathbf{O}_N is the $(N \times N)$ -null matrix and \mathbf{D} is the matrix

$$\mathbf{D} = \begin{pmatrix} -1 & 1 & 0 & \dots & 0 \\ 0 & -1 & 1 & \ddots & \vdots \\ \vdots & \ddots & \ddots & \ddots & 0 \\ 0 & \dots & 0 & -1 & 1 \\ 1 & 0 & \dots & 0 & -1 \end{pmatrix}. \quad (3.4)$$

The associated characteristic equation is

$$[\tau\lambda^2 + (\gamma + 1)\lambda + \beta]^N - (\gamma\lambda + \beta)^N = 0. \quad (3.5)$$

Notice that $\lambda = 0$ is always an eigenvalue of \mathbf{M} and that this corresponds to the presence of the conserved quantity $\sum_{k=1}^N \phi_k = L$. This very relation can be used to reduce the dimension of the system and this needs to be done for two reasons. First we will show below that the system can undergo a Hopf bifurcation but the Hopf theorem cannot be applied when the matrix of the linearized system is singular. Second numerical integration and continuation algorithms greatly gain in stability if no zero eigenvalue is present.

Since the sum of the first N equations of (3.2) gives $\sum_{k=1}^N \dot{\phi}_k = 0$ we can discard the N -th equation and eliminate the only other occurrence of ϕ_N (in the $2N$ -th equation) by setting $\phi_N = L - \sum_{k=1}^{N-1} \phi_k$. We obtain the reduced system

$$\begin{cases} \dot{\phi}_j = \psi_{j+1} - \psi_j & j = 1, \dots, N-1 \\ \dot{\psi}_j = \frac{1}{T(\phi_j)} [V(\phi_j) - \psi_j + \alpha \cdot (\psi_{j+1} - \psi_j) F(\phi_j)] & j = 1, \dots, N-1 \\ \dot{\psi}_N = \frac{1}{T(L - \sum_{k=1}^{N-1} \phi_k)} [V(L - \sum_{k=1}^{N-1} \phi_k) - \psi_N + \alpha \cdot (\psi_1 - \psi_N) F(L - \sum_{k=1}^{N-1} \phi_k)] \end{cases} \quad (3.6)$$

Linearizing system (3.6), we obtain $\dot{\mathbf{z}} = \mathbf{A}\mathbf{z}$, where $\mathbf{z} := (\phi_1 - d, \dots, \phi_{N-1} - d, \psi_1 - c, \dots, \psi_N - c)^T$ and it is easy to show that the $(2N-1) \times (2N-1)$ -

matrix \mathbf{A} has the same eigenvalues of \mathbf{M} except the zero, i.e., all the solutions of (3.5) except $\lambda = 0$.

We want to study the stability of the stationary solution when the parameters of the system are varied. The natural candidate as a bifurcation parameter would be N , but it is not suitable for this role because it is discrete and because, varying it, varies the dimension of the system itself. So we fix the value of N and let L vary instead, i.e., we imagine the circuit on which the cars move to shrink or swell. Choosing for example

$$V(x) = \frac{\tanh 2(x-1) + \tanh 2}{1 + \tanh 2}, \quad T(x) = \frac{x^2}{1+x^2}, \quad F(x) = \frac{0.5}{x+1},$$

the typical behavior of the eigenvalues of matrix \mathbf{A} (solutions of (3.5)) can be seen in Fig. 3.1, where we have plotted the curves described by the eigenvalues (in the direction shown by the arrow) as L is increased. For sufficiently small values of L all the eigenvalues have negative real part. Increasing L can cause one or more pairs of eigenvalues to cross the imaginary axis (points A_1 and A_2), so that the stationary solution is unstable and a bifurcation has taken place. A further increase leads once again to a condition of stability (points B_1 and B_2). Note that in Fig.3.1 we only drew the $N - 1$ eigenvalues that can have a positive imaginary part. There are always N eigenvalues that can never cross the imaginary axis. To study this set $\lambda = i\omega$ in (3.5) and find solutions $\omega_k = s_k\beta/\sigma_k$ and the conditions for a possible of stability (i.e., the condition for which the k -th couple of eigenvalues is purely imaginary)

$$C_k\left(\frac{L}{N}\right) := \frac{\tau\beta}{\sigma_k^2} - \frac{\gamma}{\sigma_k} = \frac{1}{1+c_k}, \quad (3.7)$$

for $k = 1, \dots, N - 1$, where $c_k := \cos(2\pi k/N)$, $\sigma_k := 1 - \gamma(c_k - 1)$. Note that the left hand side of (3.7) depends on L/N through γ , τ and β , while the right hand side only depends on N . As we will show, the only bifurcation that produces stable periodic solutions is the one corresponding to $k = 1$, which is drawn in Fig.3.2. The intersection points L_1^H and L_2^H correspond to the two crossings of the imaginary axis described above. Note that function C_1 is bell-shaped due to the assumptions made on the functions V , T and F .

This suggests that for $L = L_{1,2}^H$ the system undergoes a Hopf bifurcation and therefore periodic orbits will appear (at least locally).

Theorem 2 *If N is fixed and $L = L^H$ is such that*

$$C_1\left(\frac{L^H}{N}\right) = \frac{1}{1 + \cos \frac{2\pi}{N}} \quad (3.8)$$

holds, then system (3.6) undergoes a Hopf bifurcation.

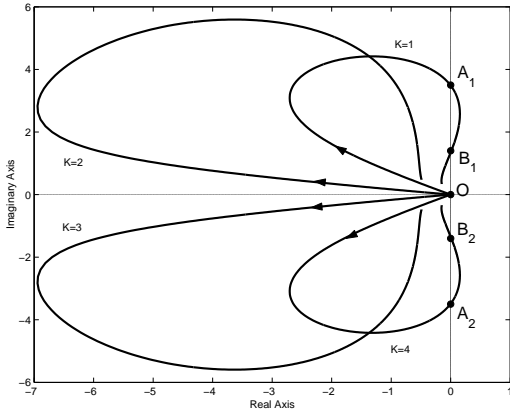


Fig. 3.1: Four of the nine eigenvalues for five cars ($N = 5$). The remaining five eigenvalues are not drawn and do not affect the stability.

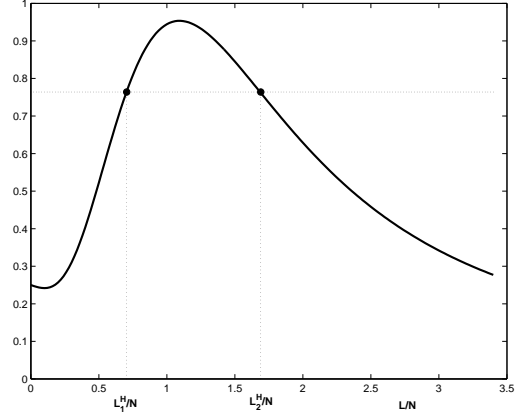


Fig. 3.2: The $C_1(\frac{L}{N})$ curve and the line $y = (1 + \cos \frac{2\pi}{N})^{-1}$ for $N = 5$.

Proof: If (3.8) is verified for some L^H , there is a solution of (3.5) $\lambda_1 := \lambda_1(L) := \mu_1(L) + i\omega_1(L)$ such that $\mu_1(L^H) = 0$. It is sufficient to prove that $\mu'(L^H) \neq 0$. This is true and it can be directly checked as in [8].

Remark 6 *It is possible to calculate the first Lyapunov coefficient of the bifurcation $l_1(L)$ (see the Appendix for this calculation and [19] for the underlying theory) and, if $l_1(L^H) \neq 0$, this can be used to gain insight in the stability of the generated periodic solutions, i.e., in sub- or super-criticality of the bifurcation.*

In the next section we show that this is the case. Note that to rigorously state that we are indeed observing a Hopf bifurcation for $L = L_{1,2}^H$ two genericity conditions must be verified. These involve long and tedious calculations, especially those relative to the Lyapunov coefficient, and are not reported here. For an example on how to proceed see [8].

Let us discuss another aspect of the conditions (3.7). Considering $\tau = \tau(L, N, \alpha)$ we can solve equation (3.7) for τ

$$\tau(L, N, \alpha) = \frac{(1 + 2\alpha F(\frac{L}{N}))[1 + \alpha F(\frac{L}{N})(1 - \cos \frac{2\pi}{N})]}{V'(\frac{L}{N})(1 + \cos \frac{2\pi}{N})} \quad (3.9)$$

For fixed N and α this is a function of L such that $\lim_{L \rightarrow 0^+} = \lim_{L \rightarrow \infty} = \infty$. In addition we have $\frac{\partial \tau}{\partial \alpha} > 0$, $\forall L, N$. This can be summarized in the

following lemma.

Lemma 5 *Aggressive driving behavior increases the stability (of the quasi-stationary solutions) in the sense that*

$$\frac{\partial \tau}{\partial \alpha} > 0, \quad \forall L, N.$$

The result of this lemma can be interpreted in two ways. The loss of stability occurs for fixed L and increasing α at higher values of τ . Alternatively we can say, that for fixed τ and increasing α the unstable region (in values of L) becomes smaller. Note that, though aggressive drivers reduce the occurrence of traffic jams, they might induce more car crashes. In fact there are investigations, where on one hand a stabilizing effect of aggressiveness and on the other hand an increased crash risk are observed [25].

3.2 Numerical bifurcation analysis

In this chapter we want to solve system (3.6) numerically with AUTO2000 (see [?]) to understand its global behavior. It is our special concern to show the dependence on different reaction times $T(x)$ and on parameter α that corresponds to the aggressiveness of the drivers. Various bifurcation diagrams will be drawn with L on the x -axis and a special norm of the solution

$$\text{Norm}(x) := \sqrt{\int_0^1 \left[\sum_{j=1}^{N-1} \phi_j(t)^2 + \sum_{k=1}^N \psi_j(t)^2 \right] dt} \quad (3.10)$$

on the y -axis with $\mathbf{x} = (\phi_1, \dots, \phi_{N-1}, \psi_1, \dots, \psi_N)^T$. In case of the stationary solution equation (3.10) becomes

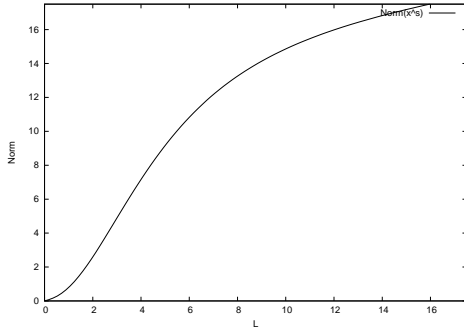
$$\text{Norm}(x) := \sqrt{\sum_{j=1}^{N-1} \left(\frac{L}{N} \right)^2 + \sum_{j=1}^N V \left(\frac{L}{N} \right)^2},$$

which is drawn in Fig. 3.3(a).

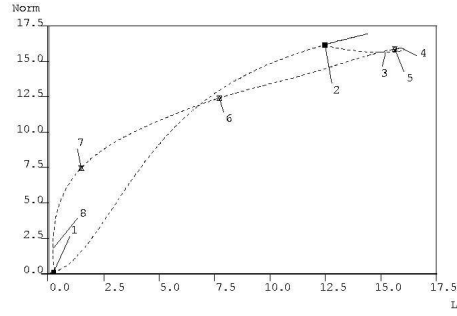
We always choose $F(x) = 0.5(x+1)^{-1}$ for the numerical analysis and use $V(x) = V_{max} \frac{x^2}{1+x^2}$ as an optimal velocity function (see [22]).

3.2.1 Aggressive drivers with constant reaction time

Let us examine the effect of the aggressive term with constant reaction times, i.e. we set $T = 1$ in (3.6). A typical bifurcation diagram for this



(a) Norm of the stationary solution.



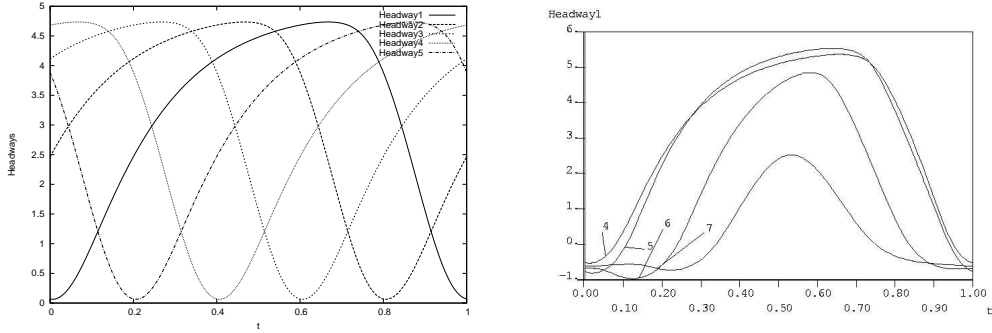
(b) Two Hopf bifurcation points (1 and 2) joined by a branch of periodic solutions.

Figure 3.3: Two Bifurcation diagrams for $N = 5$, $V^{max} = 8$ and a function $T(x) = 1$.

case is drawn in Fig. 3.3(b). What we see is the stationary solution that becomes unstable on the left (with label 1) and then stable on the right Hopf bifurcation point (label 2). These two Hopf points are joined by a branch of periodic solutions, the labels 4, 5 and 6 correspond to period doubling points, label 3 to a fold. In figure 3.4(a) we see solution 5 where all the five headways between the drivers are plotted as a function of time. One can see that the solution is a traveling wave with a phase shift of $\frac{1}{5}$ (the time is always scaled with respect to the period of the solution under consideration).

As mentioned before, there are two main aspects which need to be taken into account: the stability and the physicality of both stationary and periodic solutions. In fact most periodic solutions in figure 3.3(b) (e.g. see Fig. 3.4(b)) are *unphysical*.

Fig. 3.5 shows the influence of α on the stability of the stationary solution. The L/V_{max} -diagram shows the manifolds of the Hopf bifurcation points with varying α as a numerical result from calculations with AUTO2000. According to Lemma 5 the Hopf curve moves upward (in positive V_{max} direction) as α is increased, which means that the region in parameter space, where the stationary solution is stable, grows.



(a) The traveling wave solution corresponding to label 3 in Fig. 3.3(b).

(b) The *unphysical* solutions corresponding to labels 4, 5, 6 and 7 in Fig. 3.3(b) (one car each).

Figure 3.4: Bifurcation diagram and a periodic solution for $N = 5$, $V^{max} = 8$ and a function $T(x) = 1$.

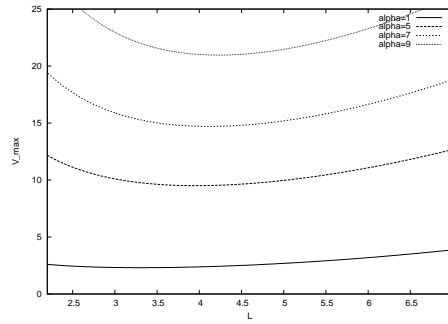
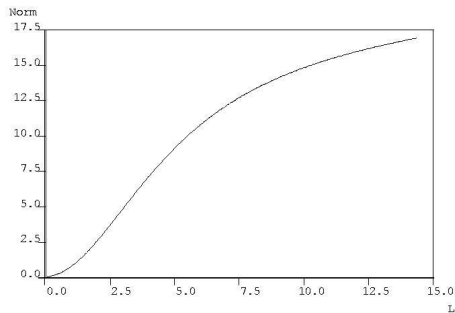


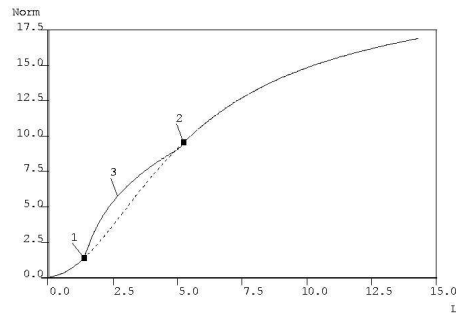
Figure 3.5: (L, V_{max}) -diagram with varying α for $N = 5$ and with (constant) function $T(x) = 1$.

3.2.2 The pure optimal velocity model with variable reaction time

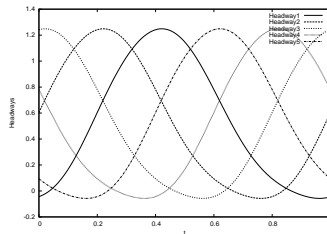
In the previous section we always chose the reaction time $T(x) = 1$. Now we want to have a look at the influence of a non-constant T on the bifurcation diagrams. In the simulations that correspond to Figs. 3.6(a) and 3.6(b) T is still constant but very small. One can see, that in the first case ($T(x) = 0.1$) there is no unstable stationary solution while in the second ($T(x) = 0.2$) the distance between the two Hopf bifurcation points, that are joined by a branch of stable periodic solutions, is small. This is what we would expect from real traffic: drivers who are quicker to react, can better absorb perturbations and find again the ordered situation corresponding to the stationary solution.



(a) $T(x) = 0.1$



(b) $T(x) = 0.2$



(c) The traveling wave corresponding to the (unphysical) solution 3 in Fig. 3.6(b)

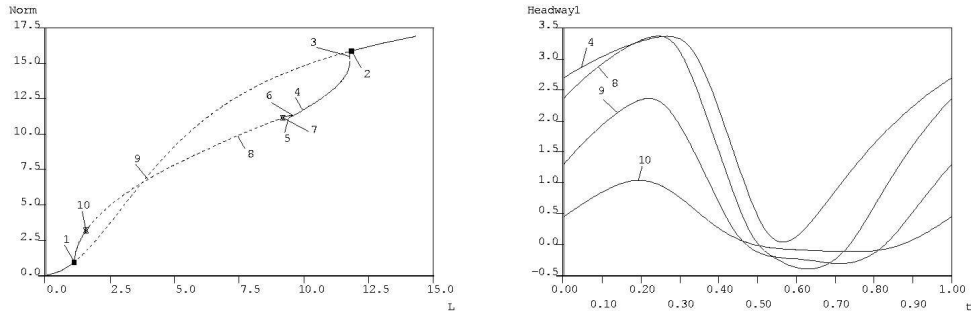
Figure 3.6: Bifurcation diagrams and a special periodic solution for $N = 5$, $V_{max} = 8$ and constant (low) $T(x)$.

From Fig. 3.6(c) it can be seen that there are still unrealistic periodic

solutions in the simulation because the headways are sometimes negative.

Next we would like to combine the previous reaction times by taking a function T that is 0.2 for small headways and 1 for big ones. This seems to be a realistic approach, because drivers become more attentive when they are closer to the car ahead.

Fig. 3.7 shows the results of the simulation with $T_1(x) = \frac{x^2}{1+x^2}0.8 + 0.2$. Again in Fig. 3.7(a), we see two Hopf bifurcation points (1, 2), two period doubling points (7, 10) and further on two folds (5,6). The area with stable periodic solutions is bigger than in Fig. 3.4 but Fig. 3.7(b) shows that solutions 8, 9, 10 are still unphysical while only the headways of solution 4 stay positive (we plotted just one headway as the solutions are always traveling waves).



(a) Two Hopf bifurcation points joined by a branch of periodic solutions.

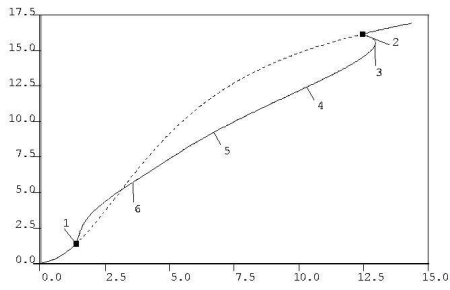
(b) Solutions corresponding to labels 4, 8, 9 and 10 in Fig. 3.7(a) projected into the evolution in time of the headway between the first two drivers.

Figure 3.7: Bifurcation diagram and periodic solutions for $N = 5$, $V^{max} = 8$ and a function $T_1(x) = \frac{x^2}{1+x^2}0.8 + 0.2$.

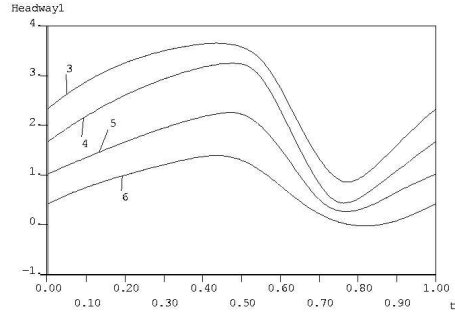
In comparison to this see Fig. 3.8 where we use the function $T_2(x) = \frac{x^6}{1+x^6}0.8 + 0.2$ as a reaction time with a faster changeover between the two different states than T_1 . It can be recognized from the fact that the headways corresponding to solutions 3, 4, 5 and 6 in Fig. 3.8(b) are positive, so it looks like the new reaction time works like a bumper between the cars.

In Fig. 3.9 three different reaction times T_1 , T_2 and T_3 can be seen where in T_3 the drivers are more watchfully for small headways than in T_1 and T_2 .

At last we want to increase the number of cars in order to see if the system behaves in a similar way as before. Therefore we choose the function



(a) Two Hopf bifurcation points joined by a branch of periodic solutions.



(b) Solutions corresponding to labels 3 to 6 in Figure 3.8(a).

Figure 3.8: Bifurcation diagram and phase space portrait of a periodic solution for $N = 5$, $V^{max} = 8$ and a function $T_2(x) = \frac{x^6}{1+x^6}0.8 + 0.2$.

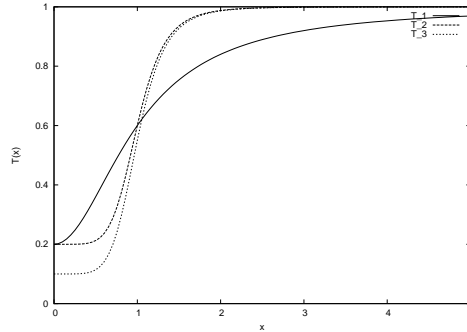
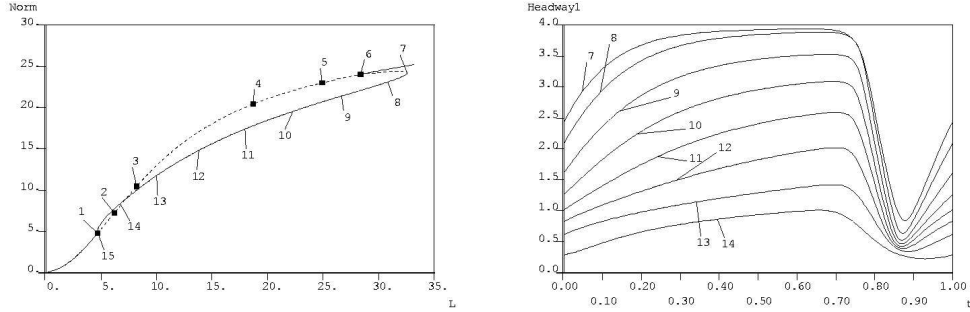


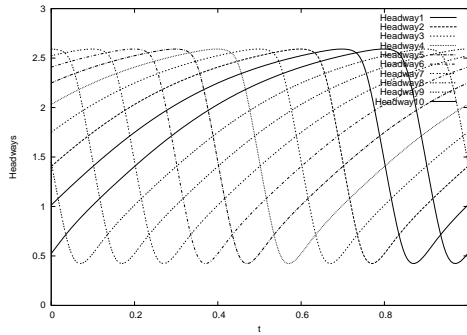
Figure 3.9: Three different functions $T_1(x) = \frac{x^2}{1+x^2}0.8 + 0.2$, $T_2(x) = \frac{x^6}{1+x^6}0.8 + 0.2$ and $T_3(x) = \frac{x^6}{1+x^6}0.9 + 0.1$.

$T_3(x) = \frac{x^6}{1+x^6}0.9 + 0.1$ as reaction time and repeat the previous simulation with ten cars.



(a) Two Hopf bifurcation points joined by a branch of periodic solutions.

(b) Solutions corresponding to labels 7 to 14 in Fig. 3.10(a).



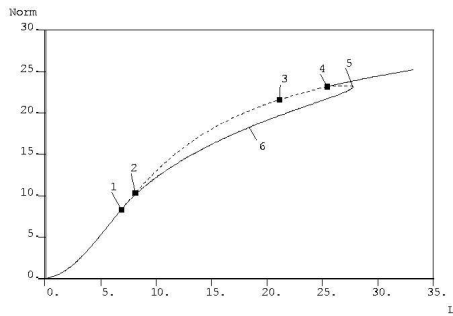
(c) Traveling wave solution corresponding to label 11 in Figure 3.10(a).

Figure 3.10: Bifurcation diagram and periodic solutions for $N = 10$, $V^{max} = 8$ and a reaction time $T_3(x) = \frac{x^6}{1+x^6}0.9 + 0.1$.

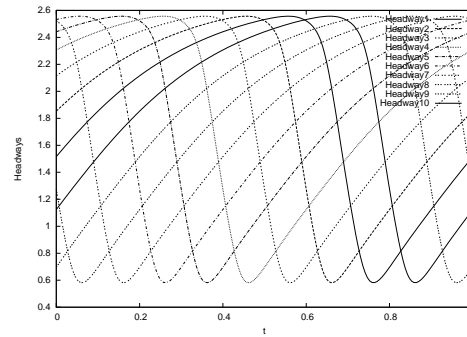
The bifurcation diagram and the phase space in figure 3.10 affirm the results from before. We now have six Hopf bifurcations (with labels 1 to 6) from which the outer, where the stationary solutions changes its stability, are the most interesting ones. Between them, the branch of periodic solutions becomes stable after a fold (solution 7). Fig. 3.10(c) shows the traveling wave of solution 11 where the ten headways of the drivers contain a phase shift of $\frac{1}{10}$ over the whole period now. There is no orbit in the branch of periodic solutions between the Hopf bifurcations that is unrealistic (Fig. 3.10(b)).

3.2.3 The full model (3.1)

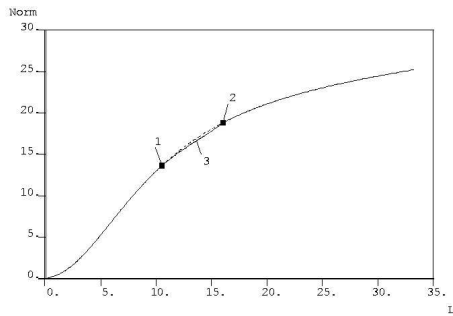
In the last section of this chapter we use both the variable reaction time T and the aggressiveness of the drivers α for parameters that might have an influence of the stability and the quality of the system concerning the unrealistic solutions. Figure 3.11 shows the effect of these two quantities.



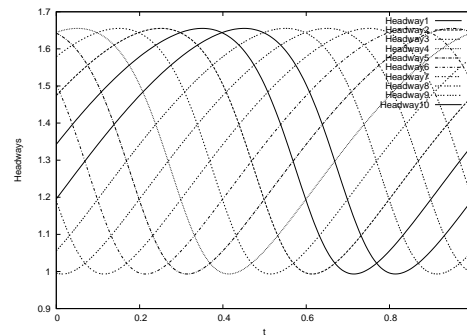
(a) $\alpha = 1$



(b) $\alpha = 1$: Traveling wave corresponding to label 6 in 3.11(a).



(c) $\alpha = 5$



(d) $\alpha = 5$: Traveling wave corresponding to label 3 in 3.11(c).

Figure 3.11: Bifurcation diagrams and phase space portrait of some periodic solutions with varying aggressiveness. $N = 10$, $V^{max} = 8$ and a function $T_3(x) = \frac{x^6}{1+x^6}0.9 + 0.1$.

One can directly compare Fig. 3.11(a) and 3.11(c) to Fig. 3.10 (where $\alpha = 0$). First we know from the starting section of this chapter and from the theoretical analysis, that an increasing α makes the system more stable in the

sense explained above. But this implicates that for a fixed V_{max} the distant between the two outer Hopf bifurcation points shrinks. Hence the bifurcating periodic solutions have a decreasing amplitude. Further more one can see from Figs. 3.10(b), 3.11(b) and 3.11(d) that the minimum of the particular traveling wave increases – in a way the solutions become more realistic.

Chapter 4

Conclusions

In this short chapter I will summarize the exposed analysis of follow-the-leader traffic models.

The most general follow-the-leader model, written in (1.3), makes assumption that the headway $x_{j+1} - x_j$ is the major quantity observed by the drivers during the motion and that the value of this quantity at any given instant, determines future changes to speed and position.

The headway appears as argument of three functions in (1.3), corresponding to the three characteristics of the sub-models analyzed in this work: the optimal velocity term $V(x_{j+1} - x_j) - y_j$, the aggressiveness term $\alpha(y_{j+1} - y_j)F(x_{j+1} - x_j)$ and the reaction time function $T(x_{j+1} - x_j)$.

Moreover system (1.3) allows for the possibility that each car would have different functions in these terms (non-equal drivers models). Models for which this is not the case are those where all the drivers obey to the same driving law (equal drivers models).

We only considered system (1.3) on a circular road.

For all the considered equal drivers models we showed that:

1. The loss of stability of quasi-stationary solutions can be shown rigorously to be due to a Hopf bifurcation. This is true for general optimal velocity functions V , aggressiveness functions F and reaction time functions T satisfying only a very few basic requirements.
2. The bifurcation is not necessarily subcritical (as conjectured in literature).
3. For the optimal velocity model we analytically obtain a criterion which tells us about the sub- or supercriticality of the Hopf bifurcation. In the case of aggressive behavior and variable reaction times it is still possible to produce such a result but it has a very complicated form.

4. Performing a numerical global bifurcation analysis we see that the critical parameter for the loss of stability obtained by the linear stability analysis is in general not the relevant one. Even in the stable regime stable periodic solutions may (co-)exist. In particular this is independent of the type of Hopf bifurcation.
5. Aggressive behavior and variable reaction time seems to favor the stability of the quasi-stationary solution.

For the non-equal drivers optimal velocity model we analytically confirmed that faster (slower) reacting cars stabilize (destabilize) the traffic flow. In addition we show that this is in general not the case if cars with different reaction times are present.

Appendix A

Calculation of a first Lyapunov coefficient

In this appendix I will go back to the situation described in section 3.1 and explicitly calculate the Lyapunov coefficient relative to the Hopf bifurcation of system (3.6). First I rewrite system (3.6) in terms of the variable $\mathbf{z} := (\xi, \eta)$ with $\xi_j := \phi_j - d$ and $\eta_j := \psi_j - c$ for $j = 1, \dots, N$ obtaining

$$\begin{cases} \dot{\xi}_j = \eta_{j+1} - \eta_j \\ \dot{\eta}_j = \frac{1}{T(\xi_j + d)} [V(\xi_j + d) - \eta_j - c + \alpha \cdot (\eta_{j+1} - \eta_j)F(\xi_j + d)] \\ \dot{\eta}_N = \frac{1}{T(d - \sum_{k=1}^{N-1} \xi_k)} [V(d - \sum_{k=1}^{N-1} \xi_k) - \eta_N - c \\ + \alpha \cdot (\eta_1 - \eta_N)F(d - \sum_{k=1}^{N-1} \xi_k)] \end{cases} \quad (\text{A.1})$$

for $j = 1, \dots, N-1$ so that now the stationary solution is $\mathbf{z}^s = \mathbf{0}$. Linearizing around \mathbf{z}^s we obtain the system $\dot{\mathbf{z}} = \mathbf{A}\mathbf{z}$, where \mathbf{A} is the following $(2N-1) \times (2N-1)$ matrix

$$\mathbf{A} = \left(\begin{array}{c|c} O_{N-1} & B_b \\ \hline \frac{\beta}{\tau} C_h & \frac{\gamma}{\tau} D - \frac{1}{\tau} I_N \end{array} \right) \quad (\text{A.2})$$

where O_{N-1} is the $(N-1) \times (N-1)$ zero-matrix, I_N is the $N \times N$ identity matrix, D is as in (3.4), B_b is the $(N-1) \times N$ matrix

$$B_b = \begin{pmatrix} -1 & 1 & 0 & \dots & 0 \\ 0 & -1 & 1 & \ddots & \vdots \\ \vdots & \ddots & \ddots & \ddots & 0 \\ 0 & \dots & 0 & -1 & 1 \end{pmatrix}. \quad (\text{A.3})$$

and C_h is the $N \times (N-1)$ matrix given by

$$C_h = \begin{pmatrix} 1 & 0 & \dots & 0 \\ 0 & \ddots & \ddots & \vdots \\ \vdots & \ddots & \ddots & 0 \\ 0 & \dots & 0 & 1 \\ -1 & \dots & \dots & -1 \end{pmatrix}. \quad (\text{A.4})$$

As already remarked, the eigenvalues of matrix \mathbf{A} are all the solutions of equation (??) except $\lambda = 0$ and this will allow us to apply the Hopf theorem and formula (2.19) for the Lyapunov coefficient.

Now fix the value of the bifurcation parameter to $L = L^H$ as in theorem 2 so that we have a single pair of eigenvalues $\pm\lambda^H := \lambda_{1,N}(L^H) = \pm i\omega$, $\omega > 0$ with zero real part while all the other eigenvalues have negative real part. We have

$$\tau^H(\lambda^H)^2 + \lambda^H = (w - 1)(\beta^H + \gamma^H \lambda^H) \quad (\text{A.5})$$

with $w := \exp(2\pi/N)$, $\tau^H := T(L^H/N)$, $\beta^H := V'(L^H/N)$ and $\gamma^H := \alpha F(L^H/N)$ or alternatively

$$\frac{\tau^H \beta^H}{\sigma^2} - \frac{\gamma^H}{\sigma} = \frac{1}{1+c}, \quad \omega = \frac{s\beta^H}{\sigma} \quad (\text{A.6})$$

where $c := \cos(2\pi/N)$, $s := \sin(2\pi/N)$ and $\sigma := 1 - \gamma^H(c - 1)$.

Note that, since the value of L is fixed to L^H throughout this appendix, there is really no need for the superscript H on parameters τ , β and γ , so I will drop them in the following. Moreover I will also write λ for λ^H , so that in the following λ is going to be the special eigenvalue of matrix (A.2) such that $\lambda = i\omega$ with ω as in (A.6).

We want to evaluate the first Lyapunov coefficient using formula

$$\begin{aligned} \ell = \frac{1}{2\omega} Re \left[& \langle \mathbf{p}, \mathbf{C}(\mathbf{q}, \mathbf{q}, \bar{\mathbf{q}}) \rangle - 2 \langle \mathbf{p}, \mathbf{B}(\mathbf{q}, \mathbf{A}^{-1}\mathbf{B}(\mathbf{q}, \bar{\mathbf{q}})) \rangle + \\ & + \langle \mathbf{p}, \mathbf{B}(\bar{\mathbf{q}}, (2i\omega_1\mathbf{I} - \mathbf{A})^{-1}\mathbf{B}(\mathbf{q}, \mathbf{q})) \rangle \right] \end{aligned} \quad (\text{A.7})$$

where \mathbf{A} is matrix (A.2) and the functionals \mathbf{B} and \mathbf{C} , defined in (2.18), are calculated for system (A.1).

I will use the following notation:

\mathbf{x} for a $(2N-1)$ column vector

\hat{x} for an $(N-1)$ column vector

\underline{x} for an N column vector

We need two vectors \mathbf{q} and \mathbf{p} such that:

$$\begin{cases} \mathbf{A}\mathbf{q} = \lambda\mathbf{q} \\ \mathbf{A}^T\mathbf{p} = -\lambda\mathbf{p} \\ \langle \mathbf{p}, \mathbf{q} \rangle = 1 \end{cases} \quad (\text{A.8})$$

Making the ansatz $\mathbf{q}^T = (\hat{q}^T, \underline{q}^T)^T$ we get

$$\mathbf{A}\mathbf{q} = \begin{pmatrix} B_b \underline{q} \\ \frac{\beta}{\tau} C_h \hat{q} - \frac{1}{\tau} \underline{q} + \frac{\gamma}{\tau \lambda} D \underline{q} \end{pmatrix} = \lambda \begin{pmatrix} \hat{q} \\ \underline{q} \end{pmatrix} \quad (\text{A.9})$$

Noting that $C_h B_b = D$, we rewrite the first equation in (A.9) as

$$D \underline{q} = \lambda C_h \hat{q} \quad (\text{A.10})$$

and plugging this into the second equation we get

$$D \underline{q} = \frac{\tau \lambda^2 + \lambda}{\beta + \gamma \lambda} \underline{q} = (w - 1) \underline{q} \quad (\text{A.11})$$

where in the second equality I used (A.5). So \underline{q} is an eigenvector of D with eigenvalue $(w - 1)$. It can be checked that $\underline{q}_k = w^k$ for $k = 1, \dots, N$ works. Now using (A.10), we discover $\hat{q}_k = \frac{1}{\lambda}(w - 1)w^k$.

Similar calculations can be used to find the adjoint eigenvector \mathbf{p} leading to

$$\mathbf{q} = \begin{pmatrix} \frac{w-1}{\lambda} \hat{u} \\ \underline{u} \end{pmatrix} \quad \mathbf{p} = \rho \begin{pmatrix} -\frac{\beta}{\tau \lambda} (\hat{u} - \hat{e}) \\ \underline{u} \end{pmatrix} \quad (\text{A.12})$$

where $\hat{u}_k = w^k, k = 1, \dots, N - 1$, $\underline{u}_k = w^k, k = 1, \dots, N$, $\hat{e}_k = 1, k = 1, \dots, N - 1$ and ρ is chosen so that $\langle \mathbf{p}, \mathbf{q} \rangle = 1$ is satisfied, i.e.

$$\bar{\rho} = \frac{1}{N} \frac{\tau \lambda^2}{\tau \lambda^2 + \beta(w - 1)} \quad (\text{A.13})$$

We now have to explicitly calculate the multilinear functions $\mathbf{B}(\mathbf{x}, \mathbf{y})$ and $\mathbf{C}(\mathbf{x}, \mathbf{y}, \mathbf{z})$ according to definitions (2.18) for system (A.1):

$$\mathbf{B}(\mathbf{x}, \mathbf{y}) = \begin{pmatrix} \hat{0} \\ \underline{B}(\mathbf{x}, \mathbf{y}) \end{pmatrix}, \quad \mathbf{C}(\mathbf{x}, \mathbf{y}, \mathbf{z}) = \begin{pmatrix} \hat{0} \\ \underline{C}(\mathbf{x}, \mathbf{y}, \mathbf{z}) \end{pmatrix} \quad (\text{A.14})$$

where $\hat{0}$ is the null $(N - 1)$ -vector,

$$\underline{B}(\mathbf{x}, \mathbf{y}) = \begin{cases} \underline{B}_k = g_1 x_k y_k + (g_2 + g_3)(x_k y_{k+N-1} + x_{k+N-1} y_k) + \\ \quad - g_3(x_k y_{k+N} + x_{k+N} y_k) \\ \underline{B}_N = g_1 \sum_{r,l=1}^{N-1} x_r y_l \\ \\ \quad - (g_2 + g_3)(y_{2N-1} \sum_{r=1}^{N-1} x_r + x_{2N-1} \sum_{r=1}^{N-1} y_r) + \\ \quad + g_3(y_N \sum_{r=1}^{N-1} x_r + x_N \sum_{r=1}^{N-1} y_r) \end{cases} \quad (\text{A.15})$$

for $k = 1, \dots, N-1$ and with coefficients g_1, g_2, g_3 representing the following quantities.

$$g_1 := \frac{1}{T^2}(V''T - 2T'V'), \quad g_2 := \frac{T'}{T^2}, \quad g_3 := -\frac{\alpha}{T^2}(TF' - FT') \quad (\text{A.16})$$

where all the functions are calculated in L^H/N . For \underline{C} we have

$$\underline{C}(\mathbf{x}, \mathbf{y}, \mathbf{z}) = \begin{cases} \underline{C}_k = d_1 x_k y_k z_k \\ \quad + (d_2 + d_3)(x_k y_k z_{k+N-1} + x_k y_{k+N-1} z_k + x_{k+N-1} y_k z_k) + \\ \quad - d_3(x_k y_k z_{k+N} + x_k y_{k+N} z_k + x_{k+N} y_k z_k) \\ \\ \underline{C}_N = -d_1 \sum_{r,l,s=1}^{N-1} x_r y_l z_s + \\ \quad + (d_2 + d_3)(z_{2N-1} \sum_{r,l=1}^{N-1} x_r y_l + y_{2N-1} \sum_{r,l=1}^{N-1} x_r z_l + x_{2N-1} \sum_{r,l=1}^{N-1} y_r z_l) + \\ \quad - d_3(z_N \sum_{r,l=1}^{N-1} x_r y_l + y_N \sum_{r,l=1}^{N-1} x_r z_l + x_N \sum_{r,l=1}^{N-1} y_r z_l) \end{cases} \quad (\text{A.17})$$

with coefficients

$$\begin{aligned} d_1 &:= -3 \frac{T''T - 2(T')^2}{T^3} V' - 3 \frac{T'}{T^2} V'' + \frac{V'''}{T} \\ d_2 &:= \frac{T''T - 2(T')^2}{T^3} V' \\ d_3 &:= \alpha \left(\frac{T''T - 2(T')^2}{T^3} F + 2 \frac{T'}{T^2} F' - \frac{F''}{T} \right) \end{aligned} \quad (\text{A.18})$$

all functions being calculated in L^H/N .

For the first term in (A.7), it can be directly checked that

$$\underline{C}(\mathbf{q}, \mathbf{q}, \bar{\mathbf{q}}) = r_1 \underline{u} \quad (\text{A.19})$$

where the constant r_1 is given by

$$\begin{aligned} r_1 &:= -\frac{d_1}{\lambda^3}(w-1)^2(w^{-1}-1) - \frac{d_2+d_3}{\lambda^2}(w-1)(2w^{-1}-w-1) + \\ &\quad + \frac{d_3}{\lambda^2}(w-1)(w^{-1}-2w+1) \end{aligned} \quad (\text{A.20})$$

so that

$$\langle \mathbf{p}, \mathbf{C}(\mathbf{q}, \mathbf{q}, \bar{\mathbf{q}}) \rangle = r_1 \langle \mathbf{p}, (\hat{O}^T, \underline{u}^T)^T \rangle = r_1 \langle \rho \underline{u}, \underline{u} \rangle = \bar{\rho} r_1 N \quad (\text{A.21})$$

The second term in (A.7) is zero. To see this notice that $\mathbf{B}(\mathbf{q}, \bar{\mathbf{q}}) = s(\hat{O}^T, \underline{e}^T)^T$ for some constant s and $\underline{e}_k = 1, k = 1, \dots, N$ and check that this is an eigenvector of matrix \mathbf{A} and consequently of matrix \mathbf{A}^{-1} , so

$$\mathbf{B}(\mathbf{q}, \mathbf{A}^{-1}\mathbf{B}(\mathbf{q}, \bar{\mathbf{q}})) \rangle = c\mathbf{B}(\mathbf{q}, (\hat{O}^T, \underline{u}^T)^T) = 0 \quad (\text{A.22})$$

As for the third term in (A.7), check first that

$$\underline{B}(\mathbf{q}, \mathbf{q}) = r_2 \underline{s}, \quad (\text{A.23})$$

where $\underline{s}_k := w^{2k}$, $k = 1, \dots, N$ and

$$r_2 := \frac{g_1}{\lambda^2}(w^2 - 1) + 2\frac{g_2}{\lambda}(w - 1) - 2\frac{g_3}{\lambda} \quad (\text{A.24})$$

so that the quantity to be calculated is $(2\lambda\mathbf{I} - \mathbf{A})^{-1}(\hat{O}^T, \underline{s}^T)^T$.

Let's set $\mathbf{L} := 2\lambda\mathbf{I} - \mathbf{A}$ and due to the structure of matrix \mathbf{A} , we can make the following ansatz

$$\mathbf{L}^{-1} = \left(\begin{array}{c|c} \tilde{L} & \tilde{B}_b \\ \hline \tilde{C}_h & \tilde{D} \end{array} \right) \quad (\text{A.25})$$

where \tilde{L} has dimension $(N-1) \times (N-1)$, \tilde{B}_b is $(N-1) \times N$, \tilde{C}_h is $N \times (N-1)$ and \tilde{D} is $N \times N$. Imposing $\mathbf{L}^{-1}\mathbf{L} = I$ we get the four relations

$$2\lambda\tilde{L} - \frac{\beta}{\tau}\tilde{B}_b\tilde{C}_h = I_{N-1} \quad (\text{A.26})$$

$$2\lambda\tilde{C}_h - \frac{\beta}{\tau}\tilde{D}\tilde{C}_h = O_h \quad (\text{A.27})$$

$$-\tilde{L}B_b + \left(\frac{1}{\tau} + 2\lambda\right)\tilde{B}_b - \frac{\gamma}{\tau}\tilde{B}_bD = 0_b \quad (\text{A.28})$$

$$-\tilde{C}_hB_b + \left(\frac{1}{\tau} + 2\lambda\right)\tilde{D} - \frac{\gamma}{\tau}\tilde{D}D = I_N \quad (\text{A.29})$$

$$(\text{A.30})$$

Note that $D\underline{s} = (w^2 - 1)\underline{s}$ and $B_b\underline{s} = (w^2 - 1)\hat{s}$. Making (A.28) act on \underline{s} we get

$$-(w^2 - 1)\tilde{L}\hat{s} + \left[\frac{1}{\tau} + 2\lambda - \frac{\gamma}{\tau}(w^2 - 1)\right]\tilde{B}_b\underline{s} = \hat{0} \quad (\text{A.31})$$

Now note that $C_h \hat{s} = \underline{s}$ and make (A.26) act on \hat{s} to get

$$2\lambda \tilde{L} \hat{s} - \frac{\beta}{\tau} \tilde{B}_{b\underline{s}} = \hat{s} \quad (\text{A.32})$$

and putting (A.31) and (A.32) together we find

$$\tilde{B}_{b\underline{s}} = h \frac{w^2 - 1}{2\lambda} \hat{s} \quad (\text{A.33})$$

where

$$h := \tau \left[1 + 2\tau\lambda - (w^2 - 1) \left(\gamma + \frac{\beta}{2\lambda} \right) \right]^{-1} \quad (\text{A.34})$$

Similarly let (A.27) act on \hat{s} and (A.29) act on \underline{s} and use the two resulting relations to get

$$\tilde{D}_{\underline{s}} = h \underline{s} \quad (\text{A.35})$$

We're interested in the quantity

$$\mathbf{L}^{-1} \begin{pmatrix} \hat{0} \\ \underline{s} \end{pmatrix} = \begin{pmatrix} \tilde{B}_{b\underline{s}} \\ \tilde{L}_{\underline{s}} \end{pmatrix} = h \begin{pmatrix} \frac{w^2-1}{2\lambda} \hat{s} \\ \underline{s} \end{pmatrix} \quad (\text{A.36})$$

so the third term in (A.7) is

$$hr_2 < \mathbf{p}, \mathbf{B}(\bar{\mathbf{q}}, \begin{pmatrix} \frac{w^2-1}{2\lambda} \hat{s} \\ \underline{s} \end{pmatrix}) > \quad (\text{A.37})$$

but

$$\mathbf{B}(\bar{\mathbf{q}}, \begin{pmatrix} \frac{w^2-1}{2\lambda} \hat{s} \\ \underline{s} \end{pmatrix}) = r_3 \begin{pmatrix} \hat{0} \\ \underline{u} \end{pmatrix} \quad (\text{A.38})$$

with

$$r_3 := -\frac{g_1}{2\lambda^2} (w^2 - 1)(w^{-1} - 1) + \frac{g_2 + g_3}{2\lambda} (2w^{-1} + w - 1) - \frac{g_3}{2\lambda} (2w^2 - w - w^{-1}) \quad (\text{A.39})$$

Plugging (A.38) in (A.37) and solving the scalar product we can write the third term in (A.7) as

$$\bar{\rho} hr_2 r_3 N \quad (\text{A.40})$$

Using now (A.21) and (A.40) in (A.7) we can write the Lyapunov coefficient for system (A.1) as

$$\ell = \text{Re} \left(\frac{r\bar{h}\omega N}{2\omega} [r_1 + hr_2r_3] \right) \quad (\text{A.41})$$

where $\bar{\rho}$ is defined in (A.13) (notice that the quantity $\bar{\rho}N$ appearing in (A.41) doesn't depend on N), h is defined in (A.34) and the quantities r_1 , r_2 and r_3 , defined in (A.20), (A.24) and (A.39) respectively, depend on the coefficients g_j and d_j ($j = 1, 2, 3$) to be found in (A.16) and (A.18).

Bibliography

- [1] A. Aw, A. Klar, T. Materne, M. Rascle, Derivation of continuum traffic flow models from microscopic follow-the-leader models, *SIAM J. Appl. Math.*, vol.63(1), pp. 259-278, 2002.
- [2] M. Bando, K. Hasebe, K. Nakanishi, A. Nakayama, Analysis of optimal velocity model with explicit delay, *Phys. Rev. E*, vol. 58, p. 5429, 1998.
- [3] M. Bando, K. Hasebe, K. Nakanishi, A. Nakayama, A. Shibata, Y. Sugiyama, Phenomenological Study of Dynamical Model of Traffic Flow, *J. Phys. I*, vol. 5, p. 1389, 1995.
- [4] M. Bando, K. Hasebe, A. Nakayama, A. Shibata, Y. Sugiyama, Structure Stability of Congestion in Traffic Dynamics, *Jpn. J. Ind. Appl. Math.*, vol. 11, p. 203, 1994.
- [5] M. Bando, K. Hasebe, A. Nakayama, A. Shibata, Y. Sugiyama, Dynamical model of traffic congestion and numerical simulation, *Phys. Rev. E*, vol. 51, p. 1035, 1995.
- [6] M. Brackstone, M. McDonald, Car Following: A Historical Review, *Transp. Res. F*, vol. 2, p. 181, 2000.
- [7] E. J. Doedel, R. C. Paffenroth, A. R. Champneys, T. F. fairgrieve, Yu. A. Kuznetzov, B. Sandstede, X. Wang, *AUTO 2000: Continuation and bifurcation software for ordinary differential equations (with Hom-Cont)*, Tech. Rep., Caltech, 2001.
- [8] I. Gasser, G. Siritto, B. Werner, Bifurcation analysis of a class of 'car following' traffic models, *Physica D*, vol. 197/3-4, pp. 222-241, 2004.
- [9] I. Gasser, T. Seidel, G. Siritto, B. Werner, Bifurcation analysis of a class of 'car following' traffic models II: variable reaction times and aggressive drivers, *Transport Theory and Statistical Physics (in publication)*, 2005.

- [10] D.C. Gazis, R. Herman, R.W. Rothery, Nonlinear follow the leader models of traffic flow, *Operations Res.*, 9, 545-567, 1961.
- [11] D. Helbing, *Verkehrsdynamik*, Springer, 1997.
- [12] D. Helbing, *Traffic and Related Self-Driven Many-Particle Systems*, *Reviews of Modern Physics*, vol. 73, pp. 1067-1141, 2001.
- [13] H.J.C. Huijberts, Improved Stability Bound for Steady State Flow in a Car-Following Model of Road Traffic on a Circular Road, *Phys. Rev. E*, vol. 65, 2002.
- [14] H.J.C. Huijberts, Analysis of a continuous car-following model for a bus route: existence, stability and bifurcation of synchronous motions, *Physica A*, vol. 308, pp. 489-517, 2002.
- [15] Y. Igarashi, K. Itoh, K. Nakanishi, K. Ogura, K. Yokokawa, Bifurcation phenomena in the optimal velocity model for traffic flow, *Phys. Rev. E*, vol. 64, 2001.
- [16] R. Illner, A. Klar, T. Materne, Vlasov-Fokker-Planck models for multi-lane traffic Flow, *Comm. Math. Sci.* 1(1), 1-12, 2003.
- [17] B.S. Kerner, *Traffic Flow: Experiment and Theory*, in M. Schreckenberg and D.E. Wolf (eds.) *Traffic and Granular Flow '97*, Springer, Singapore, 1998.
- [18] A. Klar, R.D. Kühne, R. Wegener, *Mathematical Models for Vehicular Traffic*, *Surv. Math. Ind.* 6, pp. 215-239, 1996.
- [19] Y.A. Kuznetsov, *Elements of applied bifurcation theory*, Springer, 1998.
- [20] H.K. Lee, H.W. Lee, D. Kim, Macroscopic traffic models from microscopic car-following models, *Phys. Rev. E*, vol. 64, 2001.
- [21] M.J. Lighthill, G.B. Whitham, A theory of traffic flow on long crowded roads, *Proc. Roy. Soc. A* 229, pp. 317-345, 1955.
- [22] R. Mahnke, N. Pieret, Stochastic master-equation approach to aggregation in freeway traffic, *Phys. Rev. E* vol. 56, p. 2666, 1997.
- [23] A.D. Mason, A.W. Woods, Car-following model of multispecies systems of road traffic, *Phys. Rev. E* vol. 55, p. 2203, 1997.
- [24] N. Mitarai, H. Nakanishi, Spatiotemporal structure of traffic flow in a system with an open boundary, *Phys. Rev. Lett.*, vol. 85, 2000.

- [25] L.E. Olmos, J.D. Munoz, A cellular automaton model for the traffic flow in Bogota, Int. J. Modern Physics C, 0406065, 2004.
- [26] G. Orosz, R.E. Wilson, B. Krauskopf, Global bifurcation investigation of an optimal velocity traffic model with driver reaction time, Phys. Rev. E, 70(2) 026207, 1-10, 2004.
- [27] L.A. Pipes, J. Appl. Phys. vol. 24, p. 274, 1953.
- [28] A. Reuschel, Österr. Ing.-Archiv vol. 4, p. 193, 1950.
- [29] A. Reuschel, Z. Oesterr. Ing.-Archit.-Ver. vol. 95, pp. 59-62, pp. 73-77, 1950.

Zusammenfassung

In dieser Arbeit wird der Kreisverkehr von Fahrzeugen durch einfache mikroskopische Modelle studiert. Das führt zur Analysis von großen Systemen nichtlinearer gewöhnlicher Differentialgleichungen, wobei die Größe proportional der Anzahl der Fahrzeuge ist. Die nichtlinearen Terme der Gleichungen haben die Bedeutung von *optimalen Geschwindigkeitsfunktionen* und werden heuristisch gewählt.

Es war schon in der Literatur bekannt, dass solche Systeme eine quasistationäre Lösung haben, bei der die Geschwindigkeiten und Abstände aller Fahrzeuge gleich und konstant sind. Diese spezielle Lösung kann für bestimmte Parameterwerte (z.B. der Dichte der Fahrzeuge) instabil sein und verschiedene numerische Arbeiten wiesen darauf hin, dass stattdessen stabile periodische Lösungen auftreten.

In dieser Arbeit wird analytisch bewiesen, dass der Stabilitätsverlust durch eine Hopfverzweigung zustande kommt und durch explizites Bestimmen des 1. Lyapunov Koeffizienten werden den Typ der Verzweigung und die Stabilität der lokal auftretenden periodischen Lösungen studiert.

Da diese analytische Methode nur lokale Informationen geben kann, hat man numerische Verfolgungsalgorithmen benutzt, um einen möglichst großen Ausschnitt des globalen Verzweigungsdiagramms zu erhalten. Das wichtigste Ergebnis dieser numerischen Analyse liegt in der Beobachtung, dass in manchen Parameterbereichen stabile periodische Lösungen und die stabile quasistationäre Lösung koexistieren können, so dass der durch die lineare Stabilitätsanalyse gegebene kritische Parameterwert nicht der für die Anwendung relevante ist.

Durch Störungsmethoden wurde gezeigt, dass eine Verkleinerung der Reaktionszeiten die Stabilität der quasistationären Lösung erhöht.

Die Idee einer aggressiveren Fahrweise wird auch modelliert. Das System wird dann mit einem Term erweitert, der den Versuch jedes Fahrers beschreibt, nur mehr zu einem bestimmten Anteil eine optimale Geschwindigkeit zu erreichen, sondern die Geschwindigkeit des vorderes Fahrzeuges ohne Beachtung des Abstandes. Der Vergleich der entsprechenden Verzweigungsdiagramme zeigt, dass dieses Verhalten zwar die Stabilität erhöht jedoch auch eine höhere Unfallhäufigkeit impliziert.

Summary

This work is a study of vehicular traffic on a circular road by means of simple microscopic models. This leads to the analysis of high dimensional systems of nonlinear ordinary differential equations where the size is proportional to the number of vehicles. The nonlinear terms of the equations have the meaning of *optimal velocity functions* and are heuristically chosen.

It is already in the literature that such systems have a quasi-stationary solution, in which the velocities and the headways of all the vehicles are equal and constant. This special solution can be unstable for certain parameter values (for example the value of the density of vehicles) and several numerical studies have suggested that stable periodic solutions may appear in its place.

In this work it is analytically proved that the loss of stability is due to a Hopf bifurcation, and, by explicitly determining the first Lyapunov coefficient, a study of the type of the bifurcation and of the stability of periodic solutions appearing locally is made.

Since this analytical method can only give local information, numerical continuation algorithms were used to obtain as big a part as possible of the global bifurcation diagram. The main result of this numerical analysis lies in the observation that in some parameter regions stable periodic solutions can coexist with the stable quasi-stationary solution, so that the critical values of the parameter obtained with the linear stability analysis are not relevant for the application.

Using variational methods it was shown that a decrease in the reaction times increases the stability of the quasi-stationary solution.

The idea of a more aggressive driving behavior is also modeled. The system is then enhanced with a term describing a tendency of each driver to match the speed of the driver in front rather than an optimal velocity and thus disregarding the headway.

Comparing the relative bifurcation diagram it can be seen that while this behavior increases the stability, it also makes car crashes more frequent.

Lebenslauf

Vorname: Gabriele

Nachname: Siritto

Geburtsort: Parma (Italy)

Geburtsdatum: 1. May 1975

Staatsangehörigkeit: Italian

Adresse: 83 Humber Road
Nottingham NG9 2ET
UK

E-Mail: gabriele.siritto@nottingham.ac.uk

Telefon: +44-115-84-67915 (office),
+44-7940361328 (mobile).

Vorbildung

- Aug./2005-Aug./2006 “Fellow Researcher”-Stelle am der University of Nottingham. Hauptthema: Mathematische Krebsmodelle.
- Dec./2005 Dissertation zur Erlangung des Doktorgrades mit dem Titel ”Bifurcation Analysis of a Class of Follow-the-Leader Traffic Models”.
- Jan./2002-June/2005 Stipendium beim *Graduiertenkolleg Erhaltungsprinzipien in der Modellierung und Simulation mariner, atmosphärischer und technischer Systeme*, Universität Hamburg, Department Mathematik, Hamburg. Hauptthema: “Autoverkehrsmodelle”.
- Sommer 2001 Visiting Scholar für drei Monate am *Center for Biological and Computational Learning, MIT*, Boston, USA.
- April 2001 *Laurea* (Diplom) in Theoretischen Physik am der Universität Genua, Italien. Diplomarbeit: “Statistical Learning and Game Theory”. Mit bester Note: 110/110.
- Juli 1994 Maturita’ (Abitur) an der Wissenschaftlichen Hochschule M. L. King, Genua, Italien. Mit bester Note: 60/60.